Doi link : https://doi.org/10.1039/C9RE00418A

Theoretical Study of Sensitive Reactions in Phenol Decomposition

Luna Pratali Maffei, Matteo Pelucchi, Tiziano Faravelli, and Carlo Cavallotti*

Received 00th January 20xx,
Accepted 00th January 20xx

DOI:

The reactivity of phenol is of utmost importance in combustion systems. In fact, phenol is the simplest phenolic compound, abundant in bio-oils derived from biomass fast pyrolysis and therefore included as a reference component in bio-oil surrogate mixtures. Phenol is also relevant to the mechanism of oxidation of benzene, a building block in the growth of polycyclic aromatic hydrocarbons (PAHs), precursors of soot formation. Hence, in a modular and hierarchical approach to combustion chemistry, the knowledge of the pyrolysis and combustion kinetics of phenol is essential to characterize the reactivity and the combustion properties of bio-oils and mono aromatic hydrocarbons (MAHs), as well as to improve the understanding of PAHs and soot formation. Although the reaction pathways of phenol decomposition are well defined in the literature, the rate constants still require more accurate assessment, and a validation of the reaction mechanism of phenol pyrolysis against the full set of experimental data available is still missing. In this work, we compute with the Ab Initio Transition State Theory based Master Equation (AI-TST-ME) method the rate constants of the main reaction pathways of phenol decomposition, also relevant to benzene oxidation. In particular, we investigate phenol molecular decomposition to C_5H_6 + CO and its competition with the O-H bond fission and H-atom abstraction reactions by H to form the phenoxy radical (C_6H_5O). We also investigate the successive decomposition of C_6H_5O to C_5H_5 + CO and the H-atom abstraction reaction on C_5H_6 by H, which plays a pivotal role in controlling the H concentration in phenol pyrolysis and combustion. The calculated rate constants are found to be in good agreement with experimental values. The CRECK kinetic model is updated with the new rate constants and validated against the available experimental data of phenol pyrolysis providing, to our knowledge, the first comprehensive validation of phenol decomposition kinetics. However, discrepancies are still present in the profiles of products formed from secondary reactivity. Our analysis suggests that further investigation of the reactivity of C_5H_6 is required, providing guidelines for a more accurate characterization of the decomposition to smaller species.

1. Introduction

1.1 Importance of phenol in combustion kinetics

Phenol is a compound of extreme relevance in combustion systems. Phenol and particularly the phenoxy radical play a key role as intermediates in the oxidation of benzene.[1,2] The decomposition products of phenol and phenoxy radical, C_5H_6 and C_5H_5, are essential building blocks of larger aromatic species such as indene and naphthalene,[3–7] precursors of soot and particulate matter. Phenol is also gaining attention as a reference fuel in surrogate formulations. In fact, phenol and more complex oxygenated aromatic hydrocarbons such as guaiacol, catechol, and vanillin constitute a relevant fraction (20-30% in weight) of bio-oils derived from the fast pyrolysis of lignocellulosic biomass.[8–11] Bio-oils represent a suitable near-term alternative to fossil fuels in order to reduce carbon footprint. For the above reasons, an accurate characterization of the combustion kinetics of substituted phenolic species is required in order to evaluate the technical viability of bio-oils. Phenolic compounds are included in bio-oil surrogate mixtures,[12,13] and their pyrolysis and combustion kinetics is mostly derived by analogy from the simpler chemistry of the respective mono-substituted species, namely benzene, toluene, anisole, and phenol. This requires a detailed characterization of the kinetics of phenol pyrolysis and combustion. Previous literature studies of the combustion of oxygenated aromatics underlined that, also in the presence of oxygen, the reactions relevant to pyrolysis such as molecular decomposition and H-atom abstraction by H, play a major role.[13–16] Hence, accurate rate parameters for the reaction pathways controlling phenol pyrolysis are also relevant to its oxidation. Based on analogy, improved knowledge of phenol/phenoxy kinetics is also of relevance for the extension to the oxidation of larger aromatic components (e.g. naphthalene, napthoxy radical, hydroxyl-naphthalene).

Despite the growing interest in investigating oxygenated aromatics and phenolic species, a very limited number of experimental data on the pyrolysis and oxidation of these fuels is available. In fact, phenolic compounds represent a significant experimental challenge. First, they are solid at room temperature, making their vaporization in conventional apparatuses quite complex. They are also known for their accumulation on the reactor walls, which causes difficulties even in measuring the consumption profile of the reactant.[17] Furthermore, phenol is toxic and corrosive.[18] This dearth of experimental data further justifies and supports the use of state-of-the-art theoretical methods to unravel the kinetic mechanisms and build kinetic models for the pyrolysis and oxidation of these species. To our knowledge, no extensive and systematic theoretical study of the main reactions for phenol pyrolysis is available in literature.

CRECK Modeling Lab, Department of Chemistry, Materials, and Chemical Engineering. Politecnico di Milano, Italy.
*e-mail: carlo.cavallotti@polimi.it
Electronic Supplementary Information (ESI) available. See DOI: 10.1039/x0xx00000x

1.2 State of the art on experimental and kinetic studies of phenol pyrolysis

The importance of the combustion of phenol motivates the interest towards a more fundamental understanding of its kinetics. Though the main reactions of phenol pyrolysis are well assessed, the main decomposition pathway was debated for long. In fact, the main products detected experimentally are cyclopentadiene (C_5H_6) and CO.[17,19,20] These products may form via direct molecular decomposition (r_1) or via O-H bond fission (r_2) followed by phenoxy radical decomposition to cyclopentadienyl C_5H_5 and CO (r_3), and C_5H_5 recombination with H:

$$C_6H_5OH \leftrightarrow CO + C_5H_6 \quad (r_1)$$

$$C_6H_5OH \leftrightarrow C_6H_5O + H \quad (r_2)$$

$$C_6H_5O \leftrightarrow CO + C_5H_5 \quad (r_3)$$

In the first flow reactor experiments by Lovell et al.[18] and by Manion and Louw,[21,22] performed at atmospheric pressure and 1000-1200 K, the decomposition pathway via the formation of the phenoxy radical was proposed to be dominant. However, the successive study by Brezinsky et al.[17] in the Princeton plug flow reactor (PFR) highlighted that equivalent CO and C_5H_6 profiles would be obtained assuming either of the pathways as the main one. In the same year, Horn et al.[19] performed shock tube (ST) experiments of phenol pyrolysis at high temperatures and measured CO and H profiles with resonance absorption spectroscopy. They proposed that the molecular decomposition pathway is dominant in most experimental conditions. Even in a later study, where electron paramagnetic resonance (EPR) was used for product detection, no experimental evidence was in favor of either of the two competitive C_5H_6 formation pathways.[23] This debate motivated successive theoretical studies, which confirmed the conclusion of Horn.[24,25] More recently, Scheer et al. combined theoretical calculations with experiments in a microtubular reactor, where they detected the product species with accurate techniques such as photoionization mass spectroscopy (PIMS) and matrix isolated infrared spectroscopy (IR).[26] They were able to confirm the relevance of the enol/keto tautomerization of phenol to 2,4-cyclohexadienone, the first intermediate of phenol molecular decomposition (r_1), and they confirmed that the radical decomposition pathway (r_2+r_3) is of minor importance in the investigated temperature range (475-1575 K). However, the importance of this pathway may increase at high temperatures.

In order to provide a selection of the full set of reactions contributing to the pyrolysis and oxidation of phenol and benzene, we performed sensitivity analyses with the literature CRECK kinetic model[13] at experimental conditions relevant to this system. Figure 1a) shows the sensitivity of phenol in the Princeton PFR in pyrolysis conditions (1 atm, 1173 K).[17] Other than (r_1) and (r_2), phenol consumption is also sensitive to the H-atom abstraction reaction by H on both phenol (r_4) and cyclopentadiene (r_5):

$$C_6H_5OH + H \leftrightarrow C_6H_5O + H_2 \quad (r_4)$$

$$C_5H_6 + H \leftrightarrow C_5H_5 + H_2 \quad (r_5)$$

Though (r_5) was initially neglected in the set of reactions that were theoretically investigated, its large sensitivity for H profiles in the ST reactor of Horn[19] motivated its theoretical assessment. Finally, also the ipso-addition of H on phenol to form benzene and OH radical is among the reactions contributing most to phenol consumption. This reaction is also essential in determining phenol conversion in the presence of H_2.[21] Hence, we also computed the rate constant of $C_6H_5OH + H \leftrightarrow C_6H_6 + OH$, which resulted in a similar value to that adopted in the literature CRECK mechanism.[13] Therefore, its impact on the results of the kinetic simulations was very limited. Since we are working on a systematic theoretical investigation of the ipso-addition of H on several MAHs, we will discuss this reaction in detail in a future work.

Considering that phenol is one of the main intermediates in the oxidation of benzene, we also present in Figure 1b) the sensitivity analysis of C_6H_6 consumption to rate constants in the Jet Stirred Reactor (JSR) experiments of Ristori et al. (Φ = 0.3, T = 1050 K).[27] In this case, the reactions involving the phenoxy radical play a major role, in particular phenoxy recombination with H (backward r_2) and phenoxy radical decomposition to CO (r_3). Concerning the reactivity with H radical, the H-atom abstraction (r_4) appears also in this sensitivity analysis. The reaction of the phenoxy radical with H to form cyclopentadiene and CO is implicitly included in the set of reactions studied, as it occurs via the recombination of the phenoxy radical with H to

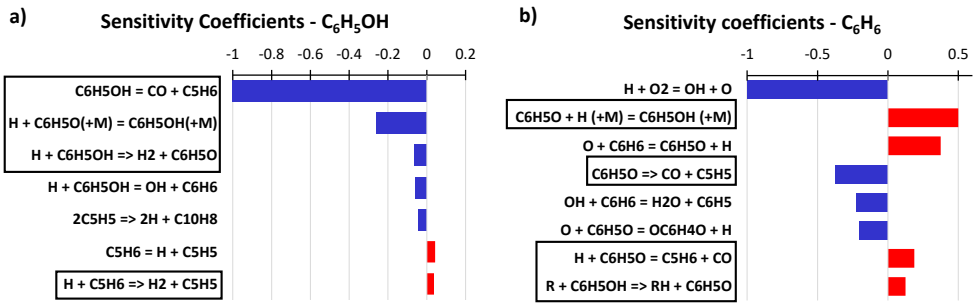

Figure 1: Sensitivity coefficients of phenol in the Princeton plug flow reactor (1173 K, 1 atm) (a) and of benzene in the jet stirred reactor experiments of Ristori et al (1050 K, Φ = 0.3) (b)

form phenol (r_2) and its successive well skipping decomposition to cyclopentadiene and CO (r_1).

In the following, we provide a summary of the state of the art of the experimental and theoretical modeling efforts for the set of reactions chosen for this study (r_{1-5}).

Phenol molecular decomposition is the most sensitive reaction in the phenol pyrolysis mechanism. The first experimental estimate of phenol decomposition rate constants ($r_{1,2}$) was conducted in the ST experiments of Horn et al. (1477-1536 K, 2.06-2.38 atm),[19] thanks to the direct measurements of H and CO profiles. A prior study of phenol hydrogenolysis in a PFR by Manion and Louw (1017-1147 K, 1 atm)[21] provided instead estimates for the r_{2-4} rates, though they considered the radical pathway for phenol decomposition to CO as the most relevant. Theoretical calculations shed light on the elementary steps of phenol molecular decomposition (r_1). The first reconstruction of the PES by Zhu and Bozzelli[24] at the CBS-QB3 level highlighted the role of the keto-enol tautomerization of phenol to 2,4-C_6H_6O (2,4-cyclohexadienone), which may stabilize in the absence of radical reactivity. This intermediate further isomerizes to the meta conformer and eventually forms cyclopentadiene via 5-member ring closure and successive decarbonylation. In this study, the authors focused on determining the enthalpies of the first step rather than a rate constant for the global reaction. In 2006, Xu and Lin[25] investigated the PES at the more accurate G2M//B3LYP/6-311G(d,p) level of theory. They also computed pressure dependent rate constants for ($r_{1,2}$) using Rice-Ramsperger-Kassel-Marcus (RRKM) theory and microcanonical variational transition state theory (VTST) for barrierless reactions at T=800-2000 K and P=0.001-100 atm. Their calculations revealed that the decarbonylation step is rate determining (with a barrier of about 75 kcal mol^{-1}). Though their rate constant for (r_1) agrees with the estimates of Horn et al.,[19] their bond fission rate constant (r_2) is about one order of magnitude lower than the estimate of Lovell et al.[18] The following experimental and theoretical study of Scheer et al.[26] highlighted that this discrepancy might be due to the missing channels of H recombination with phenoxy to form 2,4-C_6H_6O and 2,5-C_6H_6O (2,4 and 2,5-cyclohexadienone), whose C-H bond fission could contribute significantly to the formation of phenoxy radical. The PES was studied at the CBS-QB3 level and approximate rate constants were determined using QRRK theory without including variational effects. Finally, Sirjean et al.[28] computed the rate constants for (r_1) with RRKM-ME calculations in the 500-2500 K temperature range. The PES, determined at CBS-QB3 level, does not include any bond fission reaction channels. From this brief literature survey, it emerges that despite the experimental and theoretical modeling efforts to determine the kinetics of phenol decomposition, some aspects of reactions ($r_{1,2}$) are still not fully understood.

The decomposition of the phenoxy radical to cyclopentadienyl (r_3) was studied more extensively, despite the numerous experimental challenges. Phenoxy radical needs to be produced from a precursor, and the rate of reaction (r_3) is generally inferred from the resulting CO profiles. Therefore, a very low initial concentration of precursor and low pressure are required to minimize the effect of secondary reactivity. This resulted in a wide scattering of the values of the rate constant (i.e. more than one order of magnitude at 1000 K). In the first experimental study of Colussi et al.,[29] phenyl ether was selected as precursor in a Knudsen flow reactor. The authors recommended a value of about 10 s^{-1} at 1000 K. In the following ST studies of Lin and Lin,[30,31] the production of CO was investigated in a wider temperature range (1010-1430 K) at low pressure (0.5-0.9 atm). A value of around 30-60 s^{-1} at 1000 K was provided, with an activation energy of 44 kcal mol^{-1}. In the later ST study of Frank et al. (1020-1190 K, 1.3-2.5 bar),[32] this value of the activation energy was confirmed, though the measured rate was more than a factor of 3 larger than that found in the previous experimental work. They attributed this discrepancy to the smaller concentration of the allyl phenyl ether precursor, which would reduce the secondary reactivity. The most recent combined experimental and theoretical study of Shu et al.[33] was performed at similar conditions (970-1170 K, 1.4 bar) using the same precursor. They obtained a rate constant in better agreement with the experiments of Frank et al.,[32] with deviations as large as a factor of ~2. Concerning the decomposition mechanism, it proceeds via a bicyclic intermediate that forms 2,4-C_5H_5CO (2,4-cyclopentadiene carbonyl radical). 2,4-C_5H_5CO eventually decarbonylates, similarly to phenol. The first theoretical study of Olivella et al.[34] highlighted that the decarbonylation step controls the reactivity. The PES was determined at CASPT2/6-31+G(d,p)//CASSCF/6-31G(d) level, and the high pressure limit rate constant was found to be in good agreement with the data of Lin and Lin at 1000 K,[31] showing however significant deviations at high temperatures. This was explained by the first pressure-dependent theoretical study by Liu et al.[35] Though their rate constant was still considerably higher than the experimental values, their investigation of the pressure dependence revealed that already at 1000 K the rate constant enters its fall off regime at about 10 atm (about $0.8k_{inf}$, where k_{inf} is the high-pressure limit). The significant dependence on pressure also explains the activation energy of 60 kcal mol^{-1} calculated at the high-pressure limit in both theoretical studies, more than 10 kcal mol^{-1} higher than that experimentally measured. The effect of pressure was further analyzed by Carstensen et al.[36] They investigated the PES at the CBS-QB3//B3LYP/6-311G(2d,p) and CBS-QB3//QCISD/6-31G(d) levels with MP2 extrapolations to the complete basis set limit and further corrections to refine the energies of the stationary points. They computed pressure-dependent rate constants with master equation solvers that implement QRRK and RRKM theories. They confirmed that pressure effects are relevant only above 1100 K, so they concluded that the discrepancies in the available experimental data cannot be explained by the small difference in the operating pressure. Their rate constant is consistent with the experimental data of Lin and Lin and Frank et al.,[30–32] however the strong sensitivity to both the level of theory and the ME integration method did not allow to draw any conclusion on the reliability of the experimental datasets. The most recent theoretical calculations were performed by Shu et al.[33] at the G4 level of theory. In this case, the calculated

rate constant is in agreement with the experimental data they measured, being about twice the rate of Frank et al.[32] and the estimate of Carstensen et al.[36] They also point out how the energy transfer parameter $<\Delta E>_{down}$ strongly affects the final rate constants, to the point that they were able to obtain the same rate as Carstensen by increasing $<\Delta E>_{down}$ by 150 cm^{-1}. In both studies, $<\Delta E>_{down}$ was assumed to be independent on temperature. In all the mentioned theoretical studies, the temperature range of the theoretical calculations was relatively narrow (900 – 1600 K), resulting in unreliable predictions when the rate constant is extrapolated. In conclusion, none of the theoretical rate constants computed is accurate enough to be safely implemented in kinetic models to be used in a wide range of operating conditions, if the target uncertainty is smaller than a factor of 2.

Only few literature studies are available for H-atom abstraction reactions by H on phenol and cyclopentadiene ($r_{4,5}$). Due to the competition between H-atom abstraction by H and ipso-addition of H on phenol, experimental works are unable to distinguish between (r_4) and the rate constant for the H addition – beta scission reaction leading to the production of benzene and the OH radical. He et al.[37] investigated the reaction of the hydroxyl radical with phenol in a ST in the 1000-1150 K temperature range between 2.5 and 5 atm. Though they were able to quantify the overall rate for (r_4), the relatively high concentration of the H precursor and the kinetics of H recombination with phenoxy radical required the fitting of the data to a complex model, thus increasing the uncertainty of the final recommended rate constant. Manion and Louw[21] measured the profiles of the products of phenol thermolysis in H_2 in a flow reactor (922-1175 K, 1 atm). They derived the rate constants of the H-atom abstraction and H ipso-addition fitting a simple mechanism on the profiles of the main products (CO and C_6H_6). Nevertheless, they did not include phenol molecular decomposition in the mechanism, as they did not find any evidence of its contribution to CO formation. The uncertainty of the experiments and the narrow operational range of the available data encourages the support of theoretical calculations. Nevertheless, only one theoretical study of (r_4) is available in literature.[38] The PES was constructed at the MPWB1K/6-311+G(3df,2p)//MPWB1K/6-31+G(d,p) level, and the rate constants were computed using canonical VTST in the 600-1200 K temperature range. The obtained rate constant is about 3-6 times lower than the previous experimental estimates.[21,37] Finally, the contribution of H-atom abstraction by H from the ring was never addressed in literature. Only Shandross et al.[39] highlighted that the H-atom abstraction on the phenolic ring might be as relevant as that on the hydroxyl group, and assumed this rate may be two thirds that of benzene.[40]

As for H-atom abstraction by H on cyclopentadiene (r_5), no experimental measurements are available. In kinetic mechanisms, the rate constant of this reaction is often determined through analogy. The first estimate provided by Dean et al.[41] is based on H-atom abstraction on 1,3-butadiene, whereas Zhong and Bozzelli[42] considered propene as a reference, adjusting the activation energy to account for the higher exothermicity. These rates agree with the experimental estimate of Roy et al.[43] in the 1200-1600 K temperature range. However, successive theoretical calculations are in strong disagreement with these estimates, especially in terms of activation energy. Bacskay et al.[44] computed the rate constant with conventional transition state theory (TST) using RRHO in the 300-1200 K temperature range. The analysis of the PES, calculated at both CASPT2/cc-pVDZ//CASSCF/cc-pVDZ and G2(MP2)//CASSCF/cc-pVDZ levels of theory, suggested a higher apparent Arrhenius activation energy than the previous estimates (6.64 kcal mol^{-1} at the G2(MP2) level, to be compared to the 3 kcal mol^{-1} of the estimate of Dean et al.[41]). The following study of Moskaleva and Lin[45] explored the PES at the G2M(RCC,MP2)//B3LYP/6-311G(d,p) level of theory at high temperatures (1000-3000 K). They computed the rate constant using RRKM, with a $<\Delta E>_{down}$ of 200 cm^{-1}. The 0 K enthalpy of their TS is 6.34 kcal mol^{-1}, about 3 kcal mol^{-1} higher than the one computed by Bacskay et al.,[44] with a declared uncertainty of 1-2 kcal mol^{-1}. The rate constant obtained is almost one order of magnitude smaller than that of Bacskay et al.[44] Finally, the recent estimate of Nowakowska et al.[15] at the CBS-QB3 level of theory is in very good agreement (within 30% error) with the calculations of Moskaleva and Lin.[45] Because of the large discrepancies between the computed and estimated rate constants and of the significant impact of the energetics of the TS on the final rate, a revision of this rate constant at a higher level of theory is also provided in our study.

1.3 Goals of the study

The main purpose of this work is to provide accurate rate constants for reactions ($r_{1\text{-}5}$), which were identified through a preliminary sensitivity analysis as key in the mechanism of phenol pyrolysis and benzene oxidation. The final aim is developing a reliable reaction set with well-defined uncertainties suitable to be integrated in large combustion mechanisms. To accomplish this goal, theoretical calculations were performed at the highest level of theory that is possible for this system and then validated over experimental data obtained from microkinetic experiments. Then, we assessed the impact of the calculated rate constants on the modeling of phenol pyrolysis through kinetic simulations of the available experimental data. For this purpose, we update the CRECK kinetic model[13] and compare the results with the previous version. For a broader validation, we also evaluate the effect of the new rate constant in selected sets of experiments in which phenol and cyclopentadiene play a role, such as cyclopentadiene, benzene, anisole, catechol, guaiacol, and vanillin pyrolysis and oxidation (see Electronic Supporting Information-ESI). Overall, this work aims at establishing a solid and reliable basis for the development of a detailed model not only for the pyrolysis of phenol, but also for the oxidation of substituted phenolic species. The analysis of the results of the simulations also provides guidelines for further theoretical and experimental work necessary to address potentially missing reaction pathways or reactions with uncertain rate constants

that impact significantly the system kinetics, especially for what concerns the formation of secondary products.

The paper is organized as follows. In Section 2, we present an overview of the adopted theoretical methods. These include the electronic structure (ES) calculations used to construct the PESs, the methodology adopted to compute high pressure and pressure dependent rate constants, and the rationale behind the introduction of the new rate constants in the CRECK kinetic model. The results that cover the calculation of the rate constants and their impact on the kinetic model are reported in two separate sections. In Section 3, the results of the calculations of the rate constants are summarized and compared with previous literature studies. In Section 4, we describe the validation of the new model with kinetic simulations, showing the effect of our calculated rates on the global kinetic model for phenol pyrolysis. This section also presents the analysis of the results with the aim of building guidelines for the next steps in the refinement of the kinetic mechanism. Finally, in Section 5 conclusions are drawn.

2. Methods

2.1 Calculation of the rate constants

The rate constants of the selected reaction pathways were computed with ab initio transition state theory based Master Equation simulations (AI-TST-ME). The ab initio investigation of the PES was performed with EStokTP (available at https://github.com/PACChem/EStokTP),[46] an automatized software for the calculation of temperature and pressure dependent rate constants, recently developed by Politecnico di Milano and Argonne National Laboratories. EStokTP relies on external codes such as Gaussian G09[47] and Molpro 2010[48] for electronic structure calculations, and MESS for Master Equation simulations (available at https://github.com/PACChem/MESS).[49] The geometries and the vibrational frequencies at the stationary points on the PESs were computed with Density Functional Theory (DFT). In particular, for phenol and phenoxy decompositions we used the ωB97X-D functional[50] and the 6-311+g(d,p) basis set. For the H-atom abstraction reactions instead, we computed geometries and frequencies with the M06-2X functional[51] and 6-311+g(d,p) basis set, as this approach proved accurate in the calculation for H-atom abstraction reactions on similar systems.[52]

The energies of the stationary points were computed at CCSD(T)/aug-cc-pVTZ level of theory,[53] and corrected for basis set size dependence with the energy change between density fitted (DF)-MP2/aug-cc-pVQZ and DF-MP2/aug-cc-pVTZ.[54] In the ESI, also a comparison with an alternative computational protocol, where energies were computed at CCSD(T)-F12/cc-pVTZ level with core electrons and basis set corrections for the main stationary points of the PES of phenol molecular decomposition, is reported. The difference between the energies calculated at the two levels of theory is generally within 0.5 kcal/mol, which is within the energy uncertainty for the present calculations (about 1 kcal/mol on the basis of extensive comparison with experimental data in the present and previous works, if the system is not multireference).

Rate constants for H-loss barrierless decomposition pathways were evaluated using VTST, determining structures and harmonic frequencies along the minimum energy path (MEP) at the uωB97X-D/6-311+G(d,p) level and energies at the CASPT2 level.[55,56] The selected active space (AS) included 8 electrons and 8 orbitals (8e,8o), namely the 6 π and π* bonding and antibonding orbitals of the aromatic ring, and the σ and σ* bonding and antibonding orbitals of the breaking bond (O-H for phenol, and C-H for 2,4-C_6H_6O and 2,5-C_6H_6O). The energies along the MEP were computed with respect to the C_6H_5O+H adduct with the H atom positioned at 10 Å from the oxygen atom in the case of phenol and from the carbon atom in the case of 2,4-C_6H_6O and 2,5-C_6H_6O. The energies were calculated using the same AS.

For reaction pathways with relevant multi-reference (MR) character, it has been advised to use multi-reference methods when the T1 diagnostic is above about 0.02 (close-shell species) or 0.045 (open-shell species).[57] In the present study, no stationary point exhibited a T1 diagnostic larger than the reference thresholds. However, we found it was necessary to use MR methods to study properly the decarbonylation step of the molecular decomposition of phenol. In fact, despite the relatively low T1 diagnostics of 0.017, other diagnostics indicated that this step, which is a concerted process, possesses a significant multi-reference character. In particular, this was revealed by the total atomization energy (%TAE), the M diagnostics (based on the occupation of the frontier orbitals), and C_0^2 diagnostics (where C_0 is the coefficient of the Hartree-Fock determinant in the multiconfiguration expansion).[58,59] A detailed description of the multi-reference diagnostic study is reported in the ESI. The geometry and the vibrational frequencies of the TS were computed at the CASPT2/aug-cc-pVTZ level with an active space of (6e,6o), whereas for the calculation of the energies the selected active space was increased to (12e,11o). The energy change from the (6e,6o) to the (12e,11o) AS was smaller than 0.5 kcal mol^{-1}, indicating that the AS is converged with the system size. The smaller AS included the σ and σ* bonding and antibonding orbitals of the CO detaching moiety (4e,4o), and the C-C bond between the 5-membered ring and the 3-membered ring (2e,2o). In the final AS, the electrons of the π orbitals on the ring and the forming C-O π bond were also added (6e,5o). Calculations were performed using an IPEA shift of 0.25, as described by Ghigo and Roos.[60] The energy barrier was computed with respect to the reactant, whose energy was determined using the same (12e,11o) active space of the TS.

High pressure rate constants were computed treating torsional motions in the one dimensional hindered rotor approximation. The rotation potential was computed scanning the torsional angle with 20° intervals, performing the ES calculations at the same level of theory used for the geometry optimization of the stationary points.

For all reaction channels, intrinsic reaction coordinate (IRC) calculations were performed, taking 10 steps of 0.02 Å along the MEP in the direction of both reactants and products. At each

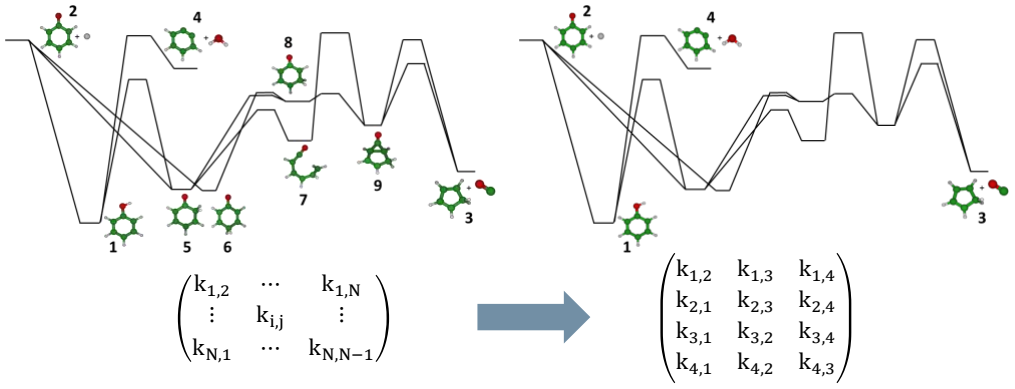

Figure 2: graphical qualitative representation of the ME-based "lumping" approach for the calculation of global rate constants for multi-well PESs.

step, the Hessian is computed and the frequencies are determined after projecting out torsional motions.[61]

For all the investigated H-atom abstraction reactions, van der Waals well structures were determined for the entrance and exit reaction channels. Accounting for van der Waals wells is useful to properly set up the Master Equation calculations, as it may account for some pressure dependence and, most importantly, allows to compute properly the energy barrier for tunneling calculations.[52] Tunneling corrections were determined using the Eckart model. [62] For most investigated reactions however, the depth of the wells was small (less than 0.5 kcal mol^{-1}), as expected in H-atom abstraction reactions by H radical. Therefore, the inclusion of van der Waals wells in the PES had only a small impact on the rate constants.

The rate constants of the reaction pathways investigated were computed in the 300–2500 K temperature and 0.1–10000 atm pressure ranges, made exception for H-atom abstraction reactions, which are pressure independent. All rate constants were computed using MESS, which solves the multi-well one-dimensional master equation with the chemically significant eigenvalues (CSEs) method using RRKM approximation, as reported in detail by Miller et al.[63] The collisional energy transfer probability is described using the exponential down model,[64] with a temperature dependent $\langle\Delta E\rangle_{down}$ of $260(T/298)^{0.875}$ cm^{-1} in an argon bath gas. All the input files for the master equation calculations are available as ESI to this paper.

The MESS code provides as output the phenomenological rate constants of the reaction pathways connecting all the stable wells on the PES, in the selected range of temperature and pressure. The rates of all elementary reaction channels were fitted with the modified Arrhenius expression as $k=AT^{n}\exp(-E_A R^{-1}T^{-1})$. The fits of the rate constants for each reaction pathway at different pressures are listed in the ESI. As regards phenol and phenoxy decomposition, we found that several of the intermediate wells considered in the PES do not stabilize in the temperature range of interest to combustion processes (above about 600 K) and, in addition, some of the wells are unlikely to exhibit a significant secondary reactivity. To decrease the number of species to include in the kinetic mechanism it was therefore decided to lump all these species into the most stable wells. Figure 2 shows qualitatively how this concept is applied to the study of the phenol decomposition PES in order to derive the global rates (r_1) and (r_2), where C_6H_5OH, C_6H_5O + H, and CO + C_5H_6 are indexed as 1, 2, 3, respectively. Shortly, the procedure adopted consists in computing at each temperature and pressure dimensionless decay profiles of the reactant (1, 2, or 3 in this example) using the phenomenological detailed kinetics obtained from MESS, considering the products as irreversible sinks. The final $k_{i,j}(T,P)$ (where i indicates the reactant and j the product) was obtained by fitting with non linear regression the exponential decay of the reactant multiplied by the branching fraction of the product j.

2.2 Kinetic simulations

We evaluated the impact of the calculated rate constants on the kinetic modeling of phenol pyrolysis through detailed kinetic simulations of the available experimental data. The operating conditions of the full set of experimental data available for phenol pyrolysis are summarized in Table 1. As highlighted in the introduction, the literature data are few and measured in a range of temperatures and pressures that is extremely narrow.

The kinetic simulations were performed using an updated version of the literature CRECK kinetic model,[13] which includes 368 species and 14332 reactions. The reactor simulations were run with OpenSMOKE++.[65] The full mechanism together with the thermodynamic and transport properties and the validation with the complete set of experimental targets are reported in the ESI.

3. Rate Constant Estimation

3.1 Phenol decomposition

The PES of phenol decomposition, determined at the level of theory described in the Methods section, is shown in Table 1. The investigated reaction channels were limited to those found

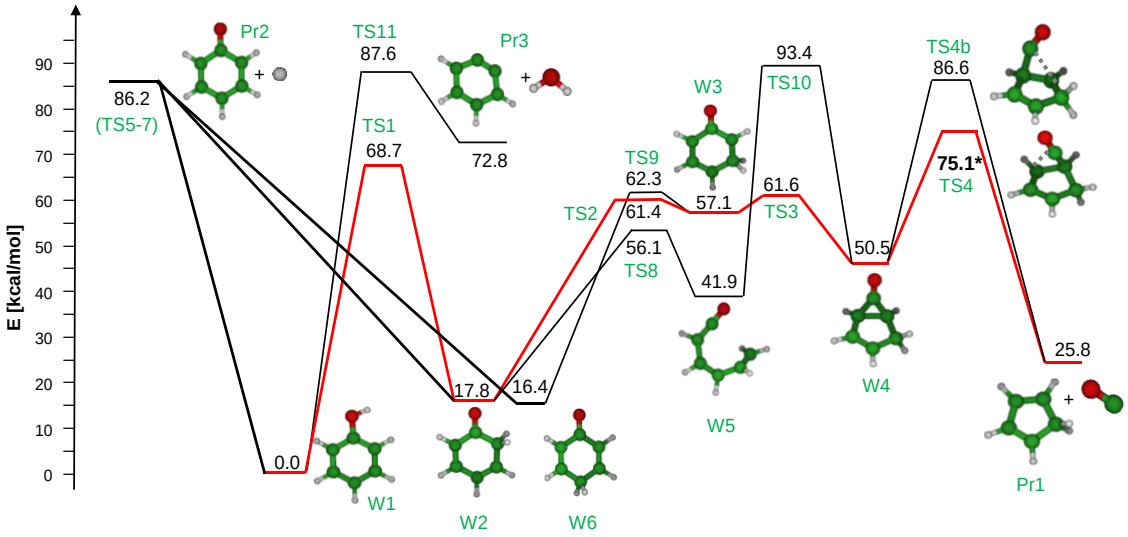

Figure 3: PES of phenol decomposition. The energies include ZPEs and were determined at the CCSD(T)/aug-cc-pVTZ//ωB97X-D/6-311+G(d,p) level, corrected for basis set effect at the DF-MP2/aug-cc-pVQZ level, made exception for the reactions marked with *, whose energies were computed with MR approaches. The main channels, marked in bold, are homolytic decomposition to phenoxy radical (black) and molecular decomposition to CO and cyclopentadiene (red).

to contribute mostly to the reactivity, as shown in previous theoretical studies of this PES.[24–26] The energies and vibrational frequencies of all stationary points are reported in the form of MESS input files in the ESI.

Phenol initial reactivity is controlled by the competition between isomerization to 2,4-cyclohexadienone (W2), with an energy barrier of 68.7 kcal mol^{-1}, and dissociation to phenoxy radical + H (Pr2). The O-H bond dissociation energy (BDE) was predicted to be 86.2 kcal mol^{-1} at 0 K, in excellent agreement with the dissociation energy of 86.5 ± 0.4 kcal mol^{-1} calculated from the ATcT tables.[66] 2,4-cyclohexadienone lies 17.9 kcal mol^{-1} higher than phenol, consistently with the 18.7 kcal mol^{-1} determined by Zhu and Bozzelli at the CBS-Q//B3LYP/6-31G(d,p) level using isodesmic reactions.[24] 2,4-cyclohexadienone can undergo C-H bond fission to form the phenoxy radical, isomerize to W3, or form through ring opening an unsaturated ketene (W5). W3 is particularly unstable due to its diradical nature, and rapidly isomerizes to either W4 or 2,5-C_6H_6O (W6). W6 lies only 16.4 kcal mol^{-1} above W1, and is about 1 kcal mol^{-1} more stable than W2, similarly to what found by Xu and Lin[25] and by Scheer et al.[26] The energy barrier between W3 and W4 (61.6 kcal mol^{-1}) is slightly smaller than that to W6 (62.3 kcal mol^{-1}). However, the latter TS is characterized by smaller vibrational frequencies, so that the reactive flux from W3 to W4 and W6 is expected to be comparable. W6 is then expected to contribute significantly to the formation of phenoxy radical, as already indicated by Scheer et al.[26] W4 can also be formed through ring closure of W5. However, the energy barrier of this channel (TS10) lies 93.4 kcal mol^{-1} above W1, so that the contribution of this pathway to the formation of W4 is minor. In a theoretical study of the same PES, Xu and Lin proposed that W5 can decompose directly to cyclopentadiene and CO.[25] In the present study we were unable to locate a similar TS, though we found a saddle point having a similar structure (TS10) that connects, as determined through an IRC analysis, W5 to W4. The intermediate W4 eventually decarbonylates to form CO + C_5H_6. As found by Xu and Lin,[25] we identified two different transition states for the final decarbonylation step (indicated as TS4 and TS4b in Figure 3. The lower-lying TS4 contributes most to the formation of CO. The energy barrier of TS4, computed at the CCSD(T)/CBS level, is 78.7 kcal mol^{-1}, thus significantly higher than the 75.8 and 74 kcal mol^{-1} determined by Xu and Lin[25] and by Scheer et al.,[26] respectively. As the present calculations are performed at a considerably higher level of theory, we consider our estimate as more representative of the energy barrier that can be computed using a single reference electronic structure computational method. W4 decomposition to cyclopentadiene is a concerted reaction, where the formation and disruption of bonds takes place contextually in a single step, as in Diels-Alder reactions. Often these reactions exhibit a significant multi-reference character. To investigate whether this was the case, we performed a thorough multi-reference diagnostics analysis, similarly to the one recently performed by Grambow et al.,[67] and described in detail in the Methods section and in the ESI. The analysis showed that, though the T1 diagnostics was relatively small, still there were significant evidences that this reaction has a non-negligible multi-reference character.

Table 1: operating conditions of the available experimetal reactor data of phenol pyrolysis.

Reactor	T [K]	P [atm]	Feed composition	Ref.
PFR	1064 – 1162	1	500 – 2016 ppm C_6H_5OH in N_2	Lovell 1989
PFR	1017 – 1147	1	[mol frac] 0.05934 C_6H_5OH, 0.02769 H_2, 0.91297 H_2O	Manion 1989
ST	1477 – 1536	2.06 – 2.38	20/24 ppm C_6H_5OH in Ar	Horn 1998
PFR	1169 – 1173	1	1004 ppm C_6H_5OH in N_2	Brezinsky 1998
PFR	945 – 1424	1.08	50 ppm C_6H_5OH in 2% H_2O and N_2	Alzueta 2000

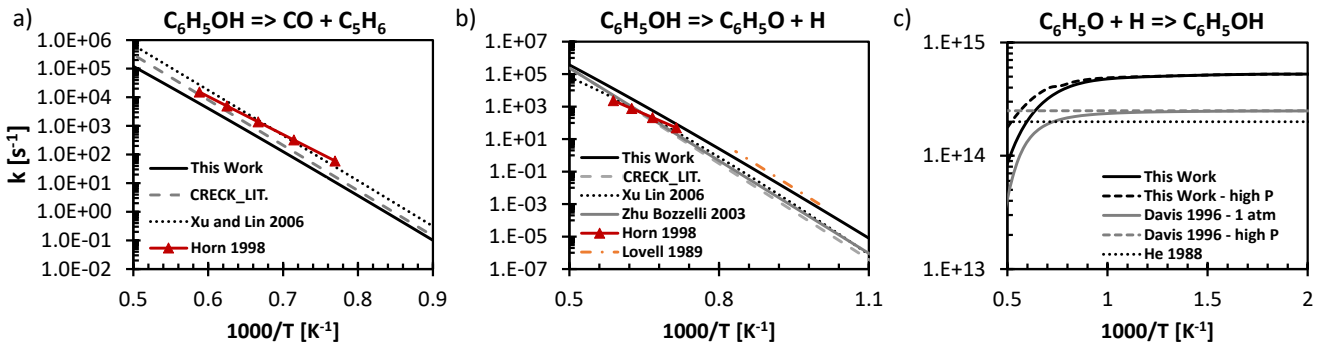

Figure 4: Global rate constants for the decomposition of phenol and comparison with available literature data.[18,19,24,25,37,68]

Because of that, we determined the energy barrier performing both geometry optimization and energy determination at the CASPT2 level, as described in detail in the Methods section. The final energy of 75.1 kcal mol^{-1} is 3.6 kcal mol^{-1} lower than that obtained at the CCSD(T) level. The impact on the rate constant is partially compensated by the higher vibrational frequencies found at the CASPT2 level with respect to those determined at the ωB97X-D level, through a sort of enthalpy-entropy compensation effect. It should be noted that the lowest vibrational frequency increases from 65.57 cm^{-1}, as determined at the ωB97X-D/6-311+G(d,p), to 116.63 cm^{-1} when calculated at the CASPT2/aug-cc-pVTZ level. To check the impact of the adopted computational protocol on the determination of the energy barrier for TS4 several additional calculations were performed, whose results are summarized in the ESI in Tables S2, S3, and S4. It was thus found that the CCSD(T) energy barrier is rather insensitive to the level at which the geometry is optimized, whether it be CASPT2 or DFT. Furthermore, the CASPT2 energy barrier decreases increasing the basis set from aug-cc-pVDZ or cc-pVTZ to the aug-cc-pVTZ level used in the present study, and the CASPT2 energies are rather well converged with the size of the active space.

Rate constants were determined solving the ME as a function of temperature and pressure, as explained in the Methods section. The Arrhenius fits of the rate constants of each reaction channel are reported in the ESI. Concerning the stabilization of the intermediate species on the PES, we found that only 2,4-C_6H_6O and 2,5-C_6H_6O exist as thermodynamically stable intermediates in an extended temperature range, even at atmospheric pressure (up until 2200 K and 1900 K, respectively). All other intermediate wells are instead stable only above 1000 atm, at temperatures lower than 1000 K. For modeling purposes, it would seem therefore appropriate to describe the reactivity of phenol in terms of conversion to W2, W6, and decomposition to the two possible reaction products: cyclopentadiene + CO and phenoxy radical + H. However, global rate constants are needed for a consistent comparison with microkinetic literature data, which normally do not account for contributions from intermediate species. It was therefore decided to use global rate constants in the updated CRECK kinetic model determined through the lumping procedure described in the Methods section, where intermediates W2 and W6 were lumped into phenol.

In Figure 4, the main global rate constants for ($r_{1,2}$) are compared with data from the literature. In each plot, we show also the rate constant adopted by the literature CRECK kinetic model (grey dashed lines). All the rate constants are at atmospheric pressure, whereas the Arrhenius parameters of the global reaction pathways at different pressures and the missing rate constants (i.e. the rates of CO + C_5H_6) are reported in the ESI. Figure 4 a) shows the results obtained for reaction (r_1). The rate constant calculated in the present work is a factor of 3-4 lower than that of Xu and Lin,[25] and differs from the experimental estimate of Horn et al.[19] by up to a factor of 4. Concerning the bond fission reaction (r_2), shown in Figure 4 b), there is good agreement with both the predictions of Xu and Lin[25] and Zhu and Bozzelli[24] and with the experimental estimate of Horn et al.[19] At lower temperatures, the estimate of Lovell et al.[18] is in better agreement with our calculations (a factor of 2-2.5) than with previous theoretical calculations (> factor of 10). Finally, the rate of recombination of H with phenoxy radical (Figure 4 c) differs by less than a factor of 2 from that obtained by the RRKM calculation of Davis et al.,[68] previously adopted by the CRECK kinetic model. The most relevant contributions to the C-H bond fission rate constant come from W2 and W6 (up to 60% and 40%, respectively).

Overall, the main difference between the present calculations and literature data consists in the lower rate found for the production of C_5H_6 and the higher one for the production of phenoxy radical. The latter is due to the contribution of intermediate species, especially 2,5-C_6H_6O (W6), which was not considered in the work of Xu and Lin.[25]

The experimental estimate of Horn et al.[19] shows some discrepancy with the current calculations. In their work, (r_1) and (r_2) were obtained fitting the CO and H profiles at different temperatures using a simplified kinetic mechanism. They assumed that (r_1) is the initial step of phenol decomposition, and the simulated CO profile was mostly sensitive to this rate.

As for (r_2), they estimated that it cannot exceed 0.15(r_1) in the investigated temperature range (1477-1536 K). However, in this work we predict that the rates of ($r_{1,2}$) are comparable in this interval, thus contradicting one of the hypotheses on which the experimental data interpretation was based. Our kinetic simulations indeed indicate that it is difficult to extrapolate a phenol decomposition rate constant from the analysis of the experimental results, as several reactions are active at the same time. This is confirmed by the fact that, despite the difference in rate constants between Horn's estimate and ours, the CO and H profiles measured in the ST experiments of Horn are in good agreement with the estimates performed using the CRECK model updated with the present rate constant estimates, as shown in Figure 5. It should be noted that the H profile is sensitive to the rate constant for H-atom abstraction on cyclopentadiene, for which we used the rate calculated in Section 3.3 of the present work. The global rate constants of the main reaction channels used to update the CRECK kinetic model are provided in Table 2 at the end of Section 3.

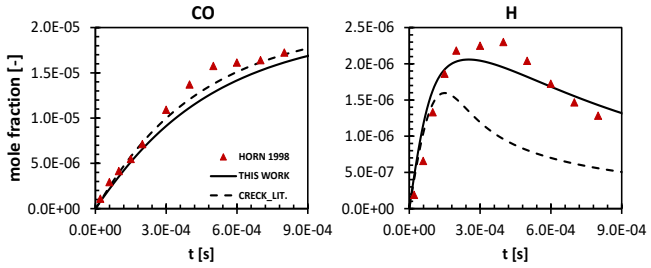

Figure 5: Profiles of CO and H in the ST reactor of Horn et al. with 20 ppm of phenol at the inlet (1536 K, 2.38 bar).[19]

3.2 Phenoxy decomposition

The PES diagram for phenoxy decomposition to cyclopentadienyl + CO and the comparison between our decomposition rate constant and literature experimental and theoretical values are shown in Figure 6. The ring opening and successive decomposition to $C_4H_3O + C_2H_2$ is not a competitive channel, given the much higher energy barriers. Hence, we only report the results for decomposition to cyclopentadienyl and CO (r_3). In the PES diagram it is also reported a comparison between the energetics of the main decomposition channel calculated in the present work with the previous theoretical estimates of Shu et al.,[33] Carstensen and Dean.,[36] and Olivella et al.[34] There is reasonable agreement with all the previous works, with a maximum discrepancy of 2.5 kcal mol^{-1} with the CBS-QB3 method. The most striking difference is the 0 K global reaction enthalpy that, though in quite good agreement with the ATcT 21.4 kcal/mol value,[66] differs by 3.5 kcal mol^{-1} from the CBS-QB3 estimate. Phenoxy decomposition involves a ring closure reaction to form a 5-membered ring (TS1), followed by the successive two steps cleavage of the two C-C bonds of the 3-membered ring (TS3, TS6). The first C-C cleavage may be considered as the rate determining step, hence it directly affects the activation energy found for the high pressure limit rate constant (53.3 kcal mol^{-1}), in good agreement with the previous calculations of Carstensen and Dean (55.2 kcal mol^{-1}).[36] The 2 kcal mol^{-1} discrepancy between our study and that of Cartesten and Dean derives from the systematic overprediction of the energy barriers that are sometimes observed at the CBS-QB3 level of theory.[69]

The calculated global decomposition rate constant is in excellent agreement with the experimental data of Frank et al.[32] (factor < 1.3) and with the recent experiments of Shu et al.[33] (factor ~2), whereas there is a larger discrepancy with the data of Lin et al.[30,31] (factor of 2-5). In the latter case the discrepancy may be attributed to the effect of secondary reactions, possibly relevant at the high phenoxy concentration of that experimental study, as already discussed in previous works and explained in the State of the art section of this paper (1.2).[32,33] As regards the theoretical rates reported in literature, we find a small discrepancy with the work of Carstensen and Dean[36] and of Shu et al.[33] in the 900-1300 K range (factor ~2). The significant difference with the rate constant of You et al. (factor of 4-7) can instead be related to the lower level of theory used, B3LYP/6-311G(d,p), which may lead to an uncertainty in the final rate constant estimation of up to one order of magnitude.[70] At high temperatures, the rate constant calculated in the present work shows a smaller decrease in the apparent activation energy with respect to the literature theoretical calculations mentioned

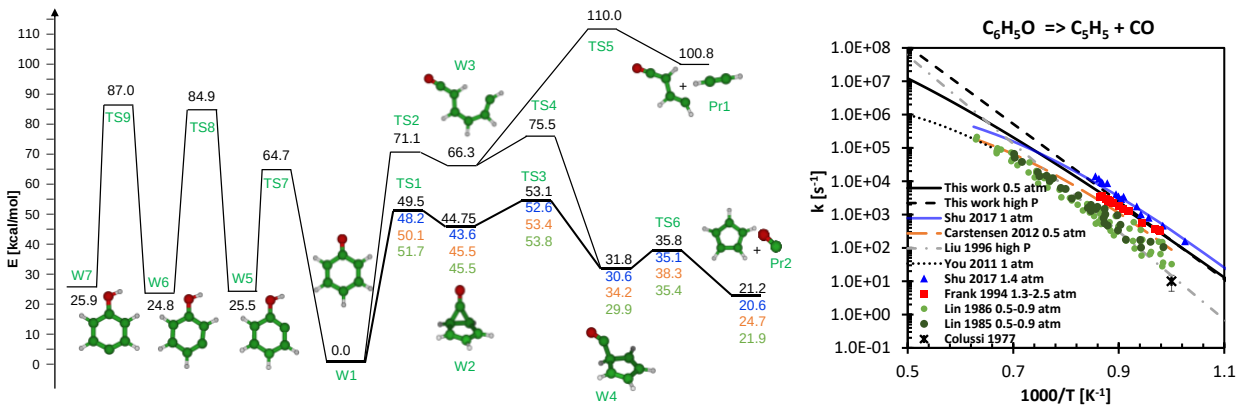

Figure 6: PES of phenoxy decomposition and corresponding rate constant, compared with previous experimental and theoretical work. Energies of the main channel are compared with other methods: G4 (Blu; Shu 2017),[33] CBS-QB3 (Orange; Carstensen 2012),[36] and CASPT2/6-31+G(d,p) (Green; Olivella 1995).[34]

above. This is probably due to the consideration of the dependence on temperature of the collisional energy transfer parameter, neglected in the previous theoretical studies. The modified Arrhenius fits for the global decomposition rate constant at different pressures are provided in Table 2.

In Figure 6, we also show on the PES the isomerization channels from the phenoxy radical to the ortho, meta, and para isomers of C_6H_4OH. None of the previous theoretical studies included them in the PES, in fact the isomerization barrier from phenoxy to o-C_6H_4OH is significantly higher than the one for decomposition (r_3). Nevertheless, when these radicals are present in the system, for instance resulting from C-H bond fission or H-atom abstraction reactions on phenol, they may either isomerize to phenoxy or decompose. In this respect, Hemberger et al.[71] conducted a combined experimental and theoretical study concerning the stability of the o,m,p-C_6H_4OH radicals. The enthalpies of both o,m,p-C_6H_4OH and the relative TSs are in reasonable agreement with the calculations of Hemberger et al.,[71] which were performed at the G3X-K level (< 0.2 kcal mol^{-1} and < 1.9 mol^{-1}, respectively). According to Hemberger et al.,[71] the ortho isomer is short-living, as it rapidly isomerizes to phenoxy, whereas the meta and para isomers may be considered as stable species in pyrolysis systems. However, they also highlighted that, as the isomerization barrier from m,p-C_6H_4OH to phenoxy lays higher than the barrier to the decomposition products, it might also be recommended to include the decompositions of m,p-C_6H_4OH to C_5H_5 + CO in kinetic models. The present ME simulations confirm the instability of o-C_6H_4OH compared to its meta and para isomers. In the ESI of this paper, we report the rate constants of the detailed unimolecular reactivity of each isomer (i.e. isomerization and decomposition to C_5H_5 + CO). However, in the kinetic simulations of the available experimental data of phenol pyrolysis we obtained equivalent results either including or excluding the unimolecular reactions of o,m,p-C_6H_4OH radicals. Furthermore, the o,m,p-C_6H_4OH radicals played no significant role in any of the conditions where phenol pyrolysis was experimentally investigated. Therefore, we conclude that, in pyrolysis conditions, phenol reactivity is well represented even if the unimolecular reactions of such isomers are omitted. Nevertheless, both isomerization and decomposition of o,m,p-C_6H_4OH radicals may be more relevant in systems with high concentrations of radicals (e.g. oxidation). Since the kinetic characterization of the oxidation of phenol and its decomposition products is beyond the scope of this work, we did not implement the unimolecular reactions of o,m,p-C_6H_4OH radicals in the updated CRECK kinetic model.

3.3 H-atom abstraction reactions by H and CH_3

In this section, we briefly discuss the results of rate constant calculations for H-atom abstraction reactions by H on phenol and cyclopentadiene. The Arrhenius fits of the computed rate constants are found in Table 2.

In Figure 7, we show the PES for H-atom abstraction by H on phenol ring in the ortho, meta, para positions, and on the OH group. The 0 K reaction enthalpy calculated for the formation of phenoxy radical + H_2 is only 0.03 kcal mol^{-1} higher than the value reported in the ATcT tables of Ruscic et al.,[66] supporting the accuracy of the adopted theoretical method for this reaction class. As expected, the energy of the TS for abstraction on OH lies about 4 kcal mol^{-1} below that for abstraction on the aromatic ring. The latter will thus become competitive with the former only at high temperatures. The comparison of the computed rate constants with the available literature data is reported in Figure 7. The experimental estimates of He et al.[37] and Manion and Louw[21] report global rate constants, thus not distinguishing H abstraction from the ring and OH. Our total rate has less than 25% discrepancy with respect to the experiments of He et al.,[37] whereas there is a larger offset with the rate proposed by Manion and Louw[21] (factor of 1.3-3.9). As explained in the previous paragraphs, this may be due to the limited set of reactions used in the kinetic model adopted to fit the experimental data. As for the rates of the single reaction channels, the abstraction by H on the OH group is comparable with the previous estimate of Zhang et al.[38] within the uncertainty of the theoretical methods used (factor < 2.3). Our total rate constant for abstraction on the ortho, meta, and para positions agrees with the estimate of Shandross et al.[39] within a factor of 2. It is noticeable that, contrary to what stated by He et al.,[37] the role of H-atom abstraction on the aromatic ring is not negligible. In fact, the rate of this reaction contributes to the total abstraction rate by 30% already at 900 K, and it becomes larger than that for abstraction on the hydroxyl group above 1300 K. In pyrolysis conditions, o-C_6H_4OH rapidly isomerizes to the phenoxy radical, therefore probably only the meta and para

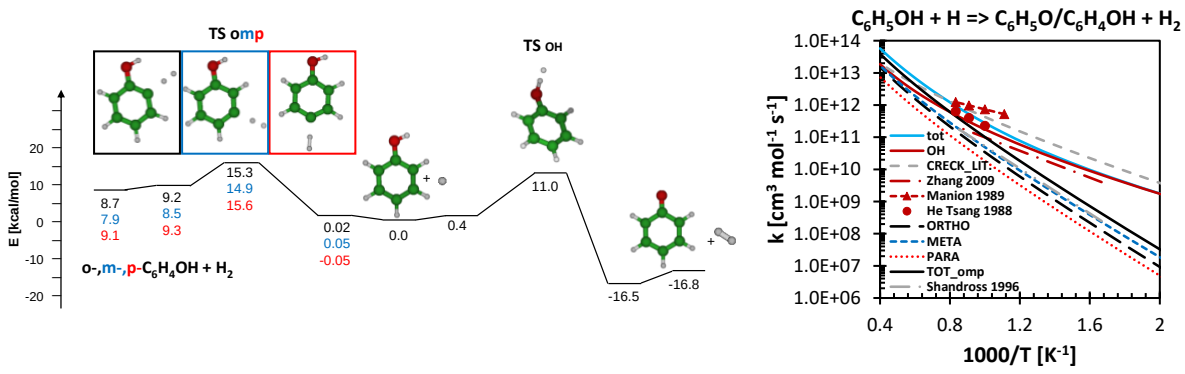

Figure 7: PES and rate constant for the H-atom abstraction by H on phenol and comparison of the rate constant with previous literature studies.[21,37-39]

isomers are thermodynamically stable at relatively low temperatures. Even in this case, H-atom abstractions on the meta and para sites on the ring account for 20% and 40% at 900 and 1800 K, respectively. In oxidation conditions instead, the isomerization of o-C_6H_4OH to phenoxy may compete with the oxidation pathways,[71,72] hence further care should be taken when studying these species in the presence of a large radical pool. Finally, we also computed the H-atom abstraction on benzene to evaluate the effect of the vicinity of the OH group. We found that the average rate of abstraction of a ring site in phenol is only slightly lower than that of the corresponding site on benzene (within a factor of 1.6). We will further investigate the effect of the vicinity of ring substitutions for H-atom abstraction reactions in future publications. It is noted that in the updated CRECK kinetic model C_6H_4OH is lumped as a single species. Hence, the global rate constant includes all the H-atom abstractions on each isomer, as explained in the following. We considered the H-atom abstractions on the OH group and on the ring in the ortho position as contributing to the formation of the phenoxy radical + H_2, assuming fast isomerization of o-C_6H_4OH to phenoxy, for the reasons explained above. The H-atom abstractions on the meta and para positions on the ring instead contribute to the formation of C_6H_4OH + H_2. The backward rate constants were then computed via thermodynamic equilibrium. To test the validity of these assumptions, we also performed kinetic simulations including the reactivity of each isomer as a separate entity, and we found no relevant change in the experimental profiles in none of the tested cases (i.e. those presented here and in the ESI). Table 2 reports the rate constants for the single channels.

In Figure 8 the PES computed for H-atom abstraction on 1,3-cyclopentadiene by H and the corresponding rate constant are presented. In this work, we did not consider the abstraction on the 1-4 sites of the ring. The 0 K reaction energy change is 0.2 kcal mol^{-1} higher than that previously computed at the G2(MP2)//CASSCF/cc-pVDZ level by Bacskay et al.,[44] and 0.6 kcal mol^{-1} lower than the calculations of Moskaleva and Lin at the G2M(RCC,MP2)//B3LYP/6-311G(d,p) level,[45] thus within the limits of the uncertainty of the theoretical methods. The TS energy of 5.6 kcal mol^{-1} is also within the 2 kcal mol^{-1} uncertainty range of the calculations of previous works. The calculated abstraction rate constant is in excellent agreement with the rate constant estimated by Sirjean et al.[73] (30% difference in the 600-2500 K temperature range). Instead, the significant discrepancy with the rate constant adopted in the literature CRECK kinetic model (factor of 5-10) explains the strong impact of this rate on systems where the H concentration is largely controlled by this reaction, as shown in the H profiles for the pyrolysis of phenol in Figure 5, and further investigated in the following section.

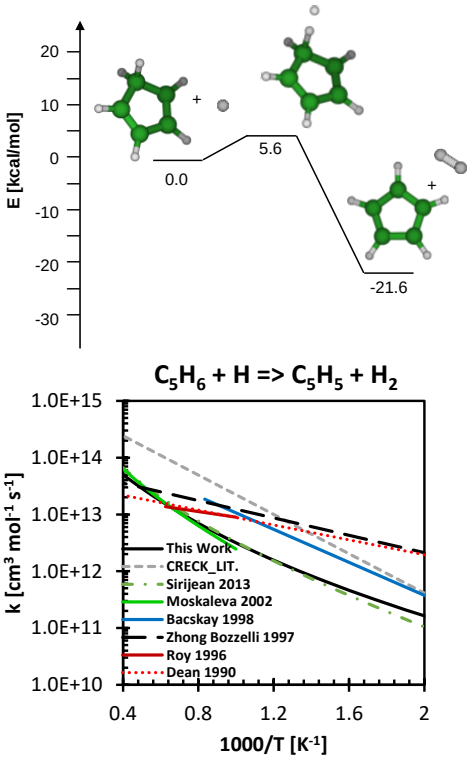

Figure 8: PES and rate constants for H-atom abstraction by H on cyclopentadiene.[41,45,72]

4. Kinetic simulations and model validation

In this section, we present the results of the kinetic simulations of phenol pyrolysis. In particular, we focus on the experimental datasets of Brezinsky et al.,[17] Horn et al.,[19] and Manion and Louw.[21] The simulations of the experimental data of Lovell et al.[18] are reported in the ESI, as they were obtained with the same reactor used for the successive experiments of Brezinsky et al.,[17] detecting however a smaller set of species. Also the simulations of the data of Alzueta et al.[20] are reported in the ESI, since we found that they were not significantly sensitive to the reactions studied in the present work. Kinetic simulations were performed also using other mechanisms reported in the literature. In particular, we present the results of the mechanism of Scheer et al.,[26] who introduced a model based on ab initio rate constants for the main reaction pathway of phenol pyrolysis (r_1). We also simulated the available data with recent kinetic mechanisms for the pyrolysis and oxidation of oxygenated aromatics, in particular the mechanisms for guaiacol oxidation of Nowakowska et al.[15] and anisole pyrolysis of Yuan et al.[74] and of Wagnon et al.[12] These all include a sub-mechanism for phenol pyrolysis.

Figure 9a) shows the profiles of the species measured in the PFR of Brezinsky et al.[17] (1173 K, 1 atm) as a function of phenol conversion. As expected, the main products of pyrolysis are CO and C_5H_6. Secondary products that were detected include benzene, and smaller decomposition products, such as methane and acetylene. Both the updated and the literature CRECK kinetic models reproduce accurately the profiles of phenol decay and of its main decomposition products, CO and C_5H_6. According to our rate of production analysis (ROPA), about 48% of phenol is consumed directly to form C_5H_6 (r_1), whereas about 26% undergoes bond fission to form phenoxy radical (r_2), which mostly decomposes to CO and C_5H_5 (r_3). C_5H_5 then recombines with H to form C_5H_6. It is remarkable that, despite

Table 2: Arrhenius fits in the form $k_0*T^{\alpha}*\exp(-EA/RT)$. Units: cal, mol, s, cm^3. The range of the Arrhenius fits is 300-2500 K, with the exception of $C_6H_5O+H=>C_6H_5OH$ and the backward rate where it was reduced to 500-2500 K.

reaction	P [atm]	k_0	α	EA	R^2
$C_6H_5OH=>CO+C_5H_6$					
	0.1	9.19E+28	-4.66	80341.64	0.9995
	1	9.30E+23	-3.12	78585.21	0.9997
	10	5.79E+21	-2.42	78075.96	0.9999
	100	3.28E+19	-1.76	77021.29	0.9999
	1000	4.88E+19	-1.80	77221.99	0.9999
	10000	1.26E+20	-1.93	77370.12	0.9999
$CO+C_5H_6=>C_6H_5OH$					
	0.1	1.84E+22	-3.44	54056.47	0.9991
	1	7.93E+16	-1.79	52171.44	0.9996
	10	2.99E+13	-0.74	50931.92	0.9998
	100	9.40E+11	-0.28	50373.33	0.9999
	1000	4.06E+11	-0.18	50226.00	0.9999
	10000	1.00E+12	-0.30	50335.40	0.9999
$C_6H_5OH=>H+C_6H_5O$					
	0.1	8.29E+48	-9.92	102202.37	0.9996
	1	6.58E+38	-6.88	97737.57	0.9998
	10	1.32E+32	-4.88	94606.07	0.9999
	100	1.14E+29	-3.97	93140.28	1.0000
	1000	2.47E+28	-3.77	92838.94	1.0000
	10000	1.79E+28	-3.73	92788.49	1.0000
$H+C_6H_5O=>C_6H_5OH$					
	0.1	2.45E+42	-8.41	11212.03	0.9245
	1	2.16E+33	-5.65	7613.88	0.9084
	10	4.11E+27	-3.92	5237.29	0.9226
	100	1.50E+25	-3.18	4210.98	0.9406
	1000	4.12E+24	-3.01	3984.37	0.9411
	10000	3.03E+24	-2.97	3936.58	0.9354
$H+C_6H_5O=>CO+C_5H_6$					**R2 of k1+k2**
	0.1	4.47E+05	2.27	873.63	0.9953
	1	1.94E+11	0.31	3493.75	0.9995
	10	3.85E+19	-12.28	-26471.03	0.9912
	100	1.03E+31	-4.84	18368.11	0.9701
	1000	1.54E+49	-9.65	29625.98	0.9728
	10000	4.74E+76	-17.62	45444.16	0.9851
duplicate					
	0.1	6.60E+35	-5.95	19123.91	
	1	7.26E+34	-5.67	18931.94	
	10	1.20E+30	-4.28	16757.75	
	100	1.17E+32	-4.84	18409.07	
	1000	5.40E+34	-17.00	-16981.85	
	10000	1.14E+26	-2.96	23880.82	
$CO+C_5H_6=>H+C_6H_5O$					
	0.1	1.09E+16	-0.72	70775.09	0.9996
	1	3.81E+19	-1.71	73650.43	0.9996
	10	4.76E+24	-3.15	76950.78	0.9998
	100	4.61E+30	-4.85	80641.99	1.0000
	1000	1.52E+33	-5.56	82224.02	1.0000
	10000	4.23E+33	-5.70	82365.49	1.0000

$C_6H_5OH=>C_6H_4+H_2O$					
	0.1	5.49E+29	-5.01	93270.62	0.9996
	1	4.36E+20	-2.19	90187.96	0.9998
	10	1.44E+15	-0.48	88549.59	1.0000
	100	3.01E+11	0.63	86988.91	1.0000
	1000	2.18E+11	0.68	87087.28	1.0000
	10000	2.10E+11	0.69	87102.55	1.0000
$C_6H_4+H_2O=>C_6H_5OH$					
	0.1	1.94E+22	-3.62	19051.58	0.9876
	1	7.12E+12	-0.70	15828.94	0.9956
	10	2.26E+06	1.30	13518.50	0.9993
	100	3.09E+03	2.17	12472.81	1.0000
	1000	7.33E+02	2.36	12241.73	1.0000
	10000	6.16E+02	2.39	12213.53	1.0000
$C_6H_5O=>CO+C_5H_5$					
	0.1	9.76E+30	-5.37	58903.48	0.9996
	1	3.44E+25	-3.62	57325.57	0.9997
	10	3.49E+21	-2.35	56114.94	0.9998
	100	5.19E+16	-0.87	54426.66	1.0000
	1000	3.51E+14	-0.20	53637.17	1.0000
	10000	9.57E+13	-0.03	53418.71	1.0000
$CO+C_5H_5=>C_6H_5O$					
	0.1	3.62E+23	-4.03	35739.16	0.9989
	1	9.87E+09	0.06	29644.99	0.9970
	10	4.52E+00	2.83	24990.59	0.9938
	100	9.56E+05	1.44	29452.80	0.9997
	1000	1.76E-07	5.10	22216.61	0.9958
	10000	1.07E-08	5.46	21627.69	0.9957
$C_6H_5OH+H=>C_6H_5O+H_2$					
	-	5.13E+00	3.80	3934.76	0.9983
$C_6H_5O+H_2=>C_6H_5OH+H$					
	-	7.10E-02	4.20	19965.74	0.9998
$C_6H_5OH+H=>o\text{-}C_6H_4OH+H_2$					
	-	2.97E+06	2.31	13135.94	1.0000
$o\text{-}C_6H_4OH+H_2=>C_6H_5OH+H$					
	-	1.29E+04	2.61	3137.21	1.0000
$C_6H_5OH+H=>m\text{-}C_6H_4OH+H_2$					
	-	5.22E+06	2.24	12564.03	1.0000
$m\text{-}C_6H_4OH+H_2=>C_6H_5OH+H$					
	-	3.94E+03	2.75	3311.29	1.0000
$C_6H_5OH+H=>p\text{-}C_6H_4OH+H_2$					
	-	4.49E+06	2.17	13321.52	1.0000
$p\text{-}C_6H_4OH+H_2=>C_6H_5OH+H$					
	-	4.18E+03	2.74	2882.17	1.0000
$C_5H_6+H=>C_5H_5+H_2$					
	-	9.02E+05	2.35	2388.54	0.9993
$C_5H_5+H_2=>C_5H_6+H$					
	-	1.70E+04	2.67	22609.43	1.0000

the updated CRECK model causes no significant change in the profiles of CO and C_5H_6, the reactive fluxes are considerably different. In fact, with the former CRECK model,[13] 74% of phenol is consumed via direct molecular decomposition, and only 13% forms phenoxy radical. This confirms the observations of Brezinsky et al.,[17] who claimed that equivalent results may be obtained by assuming either molecular decomposition or bond fission as the main consumption pathway of phenol pyrolysis. The increased concentration of phenoxy radical resulting from the updated CRECK model also leads to a higher concentration of H radicals, which can add to phenol and form benzene via ipso-addition, or abstract H from the OH group to form phenoxy. These reactions contribute to phenol consumption by 9% and 5.5%, respectively. Hence, in the updated model the amount of C_6H_6 doubles, although it still underestimates the experimental profiles.

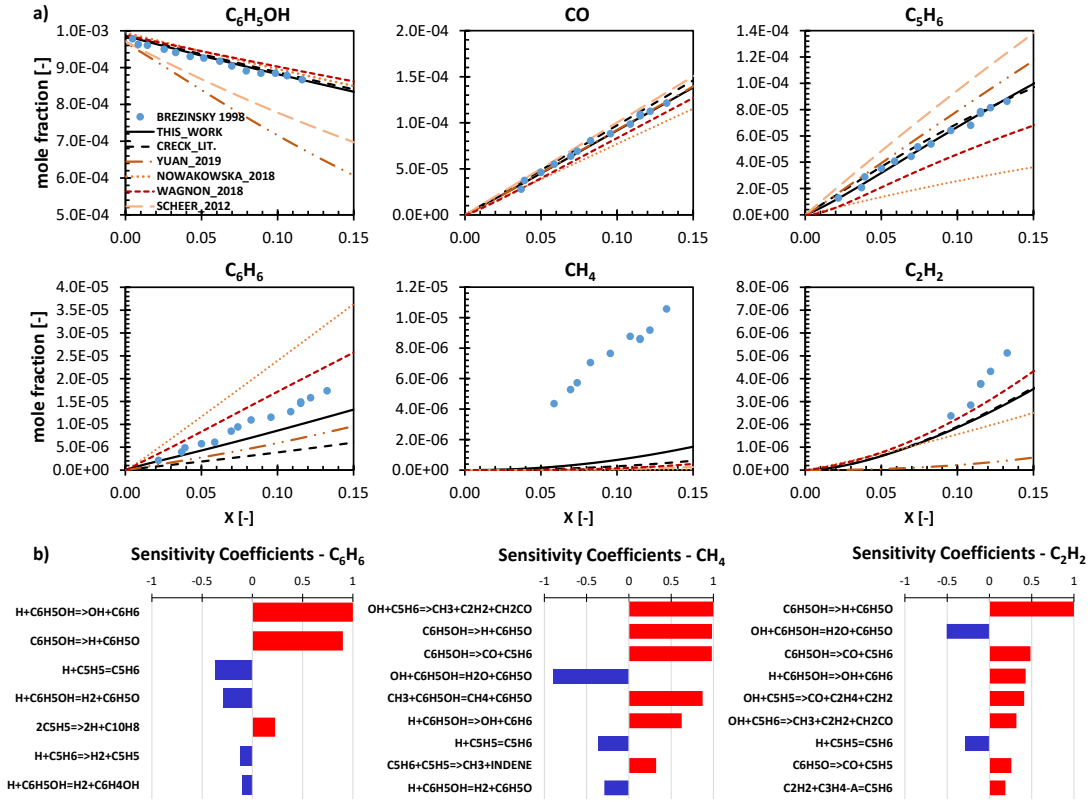

Figure 9: a) Profiles of the major species against phenol conversion measured in the PFR experiment of Brezinsky et al. (1173 K, 1 atm), b) Sensitivity analyses of C_6H_6, CH_4 and C_2H_2 in the PFR simulated with the updated CRECK mechanism.

With regards to secondary reactivity, phenoxy radical decomposes to C_5H_5, which either disproportionates to naphthalene and two hydrogen atoms, or recombines with H to form C_5H_6. A minor fraction adds to C_5H_6 to form indene and CH_3. C_5H_6 mostly converts back to C_5H_5 via H-atom abstraction reactions by H, OH and CH_3. C_5H_6 is also the main source of C_2H_2,in fact it decomposes to allene and acetylene - as also suggested by Brezinsky et al.[17] - or to methyl, acetylene, and ketene through OH addition. Finally, CH_4 is produced almost exclusively via H-atom abstraction reactions by CH_3 on both phenol (for the largest part) and cyclopentadiene.

Though the agreement between simulation results and experimental profiles of the main species is satisfactory, the model still underpredicts the fractions of both benzene and methane. Benzene is mostly produced by the ipso-addition of H on phenol, therefore it is mostly sensitive to this reaction, as shown in Figure 9b). Since H radical is the limiting reactant for benzene formation in these conditions, C_6H_6 is also sensitive to the reactions controlling the H radical pool in the system. In particular, the concentration of H radical mostly depends on the initiation reactions and H-atom abstraction reactions on phenol and cyclopentadiene. Interestingly, also the H-atom abstraction on phenol ring appears in the sensitivity analysis. In addition, Figure 9b) shows that the formation of $C_{10}H_8$ from C_5H_5 is of extreme relevance to benzene formation, due to the production of 2H. Due to the accurate characterization of phenol kinetics, we attribute the discrepancy of the C_6H_6 profile to the successive reactivity of the 5-memebered rings. Brezinsky et al.[17] suggested that a possible pathway to benzene is the recombination of CH_3 with C_5H_5 forming $CH_3C_5H_5$, which decomposes to C_6H_6 + 2H via H elimination and isomerization. Though we tested this pathway as in Lifshitz et al.,[75,76] we found it does not affect the profiles of the outlet species significantly. In fact, the concentration of the CH_3 radical is largely underpredicted, as well as that of CH_4. Methyl radical is mostly formed by the aforementioned addition of OH to C_5H_6, which is in fact the first reaction appearing in the sensitivity analysis of CH_4 shown in Figure 9b). Hence, apart from the reactions controlling phenol consumption and the formation of cyclopentadiene ($r_{1,2}$) the concentration of methane is sensitive to the reactions controlling OH and C_5H_6. In particular, the H-atom abstraction by OH on phenol, based on analogy in the literature CRECK model, was never studied theoretically in a wide range of temperatures and experimental estimates require extreme caution due to the massive secondary reactivity.[37] This suggests the need of revising this rate constant, as well as the reactivity of cyclopentadiene with OH radical. Similar conclusions can be drawn by looking at the sensitivity analysis of C_2H_2, a product of OH addition on both C_5H_6 and C_5H_5. In this case, also the reactions controlling the formation of C_5H_5 ($r_{2,3}$) appear in the sensitivity analysis.

The mechanism proposed by Scheer et al.[26] replicates the CO profile well, however it significantly overestimates the conversion of phenol, as well as the concentration of C_5H_6. This

is mostly due to the reactions of the H radical in their mechanism. In fact, they did not consider the recombination of H radical with neither phenoxy nor the C_6H_6O isomers (W2, W6 in Figure 3). This causes phenol overconsumption. Nevertheless, the CO profile as a function of conversion agrees with the experimental data, supporting the validity of their calculations as concerns the molecular decomposition pathway. Looking at the profiles obtained using the mechanism of Yuan et al.,[74] the high conversion of phenol is caused by both the high global rate constant of phenol molecular decomposition (from Xu and Lin[25]) and by the high H-atom abstraction on phenol by C_5H_5 (from Lovell et al.[18]). Nevertheless, the model reproduces reasonably the profiles of CO and C_5H_6 as a function of conversion. Interestingly, the reactivity of C_5H_6 is mostly controlled by the addition of H and the successive ring opening, which also controls the H concentration in the system. The concentration of benzene is underestimated, similarly to the CRECK model. The mechanism of Nowakowska et al.[15] well reproduces the conversion of phenol. However, the reactant is mostly consumed by H-atom abstraction reactions, in particular by OH (from Shandross et al.[39]) and by C_5H_5 (from Lovell et al.[18]). In fact, the production of C_5H_6 by molecular decomposition of phenol is lower than in the previous models. This results in a low concentration of C_5H_6, hence H radical mostly adds to phenol to form C_6H_6, which is in fact overpredicted. The model of Wagnon et al.[12] produces similar profiles to those obtained with the mechanism of Nowakowska et al.,[15] however the discrepancy with the experimental data is smaller. Interestingly, benzene is mostly produced directly from phenol decomposing to benzene + O, and partially by the H ipso-addition reaction on phenol. The underestimation of C_5H_6 is possibly due to the mechanism of phenol molecular decomposition (adopted from Sirjean et al.[28]), and by the high concentration of H produced also by the initiation reactions of W2 and W6 (estimated in their model).

In Figure 10a,b), we present the profiles of CO and H of the ST experiments of Horn et al.[19] in comparison with the literature mechanisms listed above. The two cases shown correspond to two different inlet temperatures: case a) 1536 K, case b) 1477 K. The updated CRECK model satisfactorily reproduces the profiles in both cases. Phenol is consumed mostly by (r_2) (55% and 44% for case a) and b), respectively) and by (r_1) (39% and 35% for case a) and b), respectively). The remaining fraction is consumed by the H ipso-addition reaction and by the H-atom abstraction on OH (r_4). The phenoxy radical then decomposes to CO + C_5H_5 (r_3). At lower temperatures (case b), the H concentration is slightly underestimated by the model. In fact, the H bond fission is slower than in case a). The sensitivity analysis of Figure 10c) shows the reactions controlling CO and H profiles in the first part of the reactor, where the experimental trends are well reproduced (0-3*10^{-4} s), compared to the second part of the reactor (3-9*10^{-4} s). In the case of H radical, (r_2) is the most sensitive reaction in the whole reactor. At longer residence times, H consumption is governed by ($r_{4,5}$), by H ipso-addition on phenol, and by H recombination with cyclopentadienyl radical (adopted from Harding et al.[77]).

As anticipated in Section 3, the improvement in the CRECK model with respect to the literature version is attributed to the

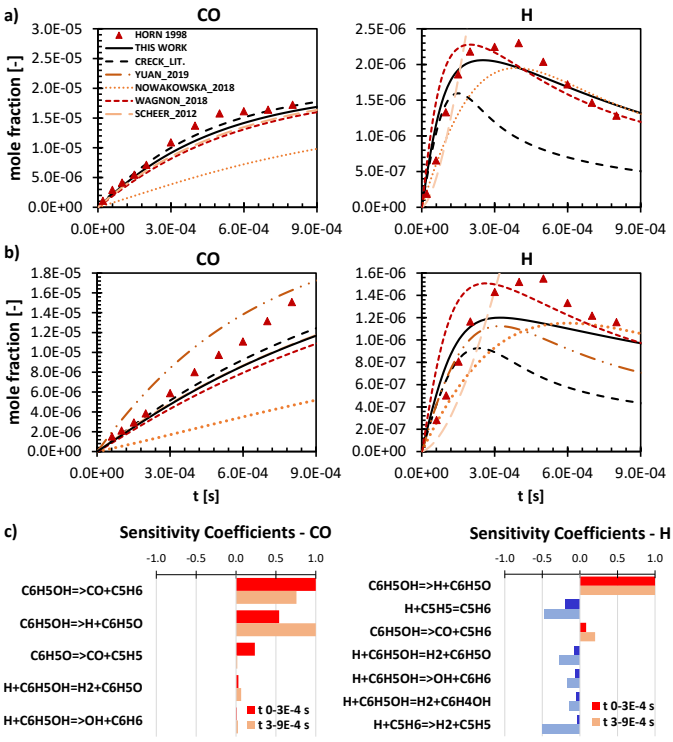

Figure 10: Profiles of CO and H of the ST experiments of Horn et al. with a) 20 ppm inlet phenol (2.38 bar, 1536 K) and b) 24 ppm phenol inlet (2.06 bar, 1477 K). The sensitivity analyses of CO and H in the first part (0-3*10^{-4} s) and in the second part (3-9*10^{-4} s) of the ST simulations with 24 ppm phenol inlet are shown in part c).

increased bond fission reaction of phenol, due to the contributions of intermediates W2 and W6, as also confirmed by the sensitivity analysis (Figure 10c). Additionally, H consumption is slower than in the previous model due to the significant decrease of the H-atom abstraction by H on C_5H_6, in particular for case a). As regards CO, Figure 10c) shows that its concentration is sensitive to all the reactions investigated. The small decrease in CO concentration compared to the previous version can only be explained by the slight decrease in (r_1) compared to the literature CRECK mechanism,[13] not compensated by the increase in the O-H bond fission to form phenoxy radical (r_2).

The mechanism of Wagnon et al.[12] performs reasonably well with respect to both species. Interestingly, CO is entirely produced by the decomposition of phenoxy radical (r_3), as the O-H and C-H bond fissions of phenol, and W2 dominates the reactivity. This is also evident from the concentration of H, which increases rapidly and anticipates slightly the experimental peak. Its consumption is regulated by the H ipso-addition and H-atom abstraction by H on phenol. Contrary to the CRECK mechanism, the reactivity of C_5H_6 is irrelevant at these conditions. The CO profile is reasonably reproduced also by the mechanism of Scheer et al.,[26] similarly to the previous case. The lack of H consumption reactions is instead evident in the final profiles. The mechanism of Nowakowska et al.[15] shows the opposite behavior: despite the underprediction of CO attributed to the low molecular decomposition of phenol, the shape of the H profile is in accordance with experiments. The H concentration in this case is controlled by O-H and C-H bond

fissions and H-atom abstraction reactions of C_6H_5OH and C_5H_6. The mechanism of Yuan et al.[74] slightly overpredicts CO due to the reasons mentioned above. The overall H concentration is underestimated, however the shape of the profile is well reproduced. Besides the bond fissions and the H-atom abstractions of C_6H_5OH and C_5H_6, also the bond fission of W2, the H ipso-addition on C_6H_5OH, and the formation of C_5H_7 from H + C_5H_6 control the concentration of H.

In Figure 11a), we present the results obtained for the species detected in the PFR experiments of Manion and Louw (1017-1147 K, 1 atm).[21] The experimental conditions differ substantially from the previous data sets, since the thermolysis of phenol occurs in the presence of hydrogen. Hence, the interaction of phenol with H and the rate constants of the backward H-atom abstraction reactions on the species in the mechanism are essential in controlling the reactivity of the system. The species profiles are reported in terms of carbon selectivity. The first experimental point shows some inconsistency with the global data set since the total carbon selectivity is about 125%, whereas for the other points it sums to 75-90%.

In the presence of H_2, phenol mostly converts to C_6H_6, CO, and C_5H_6. Compared to pyrolysis in the absence of hydrogen, small products such as C_2H_4 and CH_4 gain relevance. In this experiment, also larger aromatics such as naphthalene ($C_{10}H_8$), indene (C_9H_8), phenantrene ($C_{14}H_{10}$), and fluorene ($C_{13}H_{10}$) were measured. These derive from addition and recombination reactions of smaller rings, which are even more relevant in conditions of pure pyrolysis.

The updated CRECK kinetic model reproduces reasonably well the general trends of the experimental data, though the model performs slightly worse than the previous version, mostly due to the increased conversion of phenol. It is noted that this is not only due to the current updates to the model, but also to other modifications that are typical in the development and maintenance of a single comprehensive kinetic model, including the H-atom abstraction reaction on C_6H_6 (from Frenklach et al.[78]) and the H bond fission of C_5H_6 (from Harding et al.[77]), which are essential to the reactivity at these conditions. According to our ROP analysis, the main reaction causing phenol consumption is the H ipso-addition reaction, together with the H-atom abstraction by H (r_4) and OH radicals and molecular decomposition (r_1), which is the main source of CO. At high temperatures, also the bond fission of phenol contributes to its decomposition, and therefore to CO production via (r_3). According to our sensitivity analysis, shown in Figure 11b) for different temperatures (1030 K, 1080 K and 1130 K), the increase in phenol conversion in the updated model is mostly due to the increased bond fission of phenol (r_2) and decomposition of phenoxy radical (r_3). At higher conversion, the decrease in the H-atom abstraction on C_5H_6 significantly contributes to the increase of phenol consumption. This reaction does not remove as much hydrogen as in the previous CRECK mechanism, thus H reacts with phenol. The main product, C_6H_6, is produced by the H ipso-addition reaction on phenol, and it is partially consumed by the addition reactions to C_5H_6 and C_5H_5 to produce larger aromatics ($C_{10}H_8$, C_9H_8). At high temperatures, also the H-atom abstraction on C_5H_6 becomes relevant, together with the addition of H to indene which then decomposes to mono aromatic rings and $C_{2\text{-}3}$ species. The main reactions controlling the shape of benzene profiles are those determining the H concentration in the system, namely the H ipso-addition on phenol, and the H-atom abstractions and bond fissions of both phenol and cyclopentadiene. This is highlighted by the sensitivity analysis in Figure 11b). Despite no significant difference is observed among the temperatures considered, the sensitivity coefficients of the H-atom abstraction reactions increase with temperature, as expected.

The reactions forming and decomposing the 5-membered rings C_5H_5 and C_5H_6 and their interaction with hydrogen are essential in controlling the reactivity of the system. C_5H_6 is produced by both (r_1) and (r_5) at low conversion, whereas at higher conversion (lower H_2 concentration) also the recombination of H with C_5H_5 becomes relevant. H-atom abstraction by OH and the reaction with H_2 to form C_5H_8 consume cyclopentadiene. At high temperatures, also the reaction with C_5H_5 to form indene drains C_5H_6 significantly. C_5H_5, at low conversion, is mostly formed from the decomposition of phenoxy, and is partially consumed by (r_5) to produce C_5H_6. When the concentration of H_2 decreases, the recombination of C_5H_5 with H becomes essential in controlling the production of C_5H_6. The competition between the above mentioned pathways, H-atom abstraction, H bond fission, production via (r_3), and consumption to larger aromatics determine the shape of the profile of cyclopentadienyl. As a result, the concentration of C_5H_5 shows a peak around 1100 K, which is mirrored in the concentrations of $C_{10}H_8$ and C_9H_8. In fact, naphthalene and indene derive from addition or recombination reactions between C_5H_6, C_5H_5, and C_6H_6. The strong interlink between C_5H_5 and $C_{10}H_8$ is highlighted by the sensitivity analysis shown in Figure 11b). The reactions of formation of the phenoxy radical (r_2) and its decomposition to cyclopentadienyl (r_3) have in fact the highest sensitivity coefficients. The other relevant reactions are mainly those controlling the concentrations of H, C_5H_6, and C_5H_5, as explained above. $C_{10}H_8$ and C_9H_8 are both consumed by reactions with H to various decomposition products, including smaller aromatics (C_6H_6, C_7H_8, $C_6H_5C_2H_3$) and C_1-C_3 species (CH_4, C_2H_2, C_3H_4). C_7H_8 and $C_6H_5C_2H_3$ are then consumed with analogue H-addition reactions followed by decomposition (e.g. C_6H_6 + CH_3) and ring opening to form smaller products. Naphthalene and indene may also react further with C_5H_6 and C_5H_5 to form larger aromatic species, namely $C_{14}H_{10}$ and $C_{13}H_{10}$. Finally, biphenyl ($C_{12}H_{10}$) is produced by C_6H_5 + C_6H_6, and by H_2 + $C_{12}H_9$, in turn deriving from H + fluorene. Hence, its overestimation with respect to the experiments is due to the high concentrations of C_6H_6 and H at higher conversions.

The $C_{1\text{-}3}$ products derive from the addition reactions of H and OH to C_5H_6 and C_5H_5, causing ring-opening and successive decomposition. A minor fraction is also formed as secondary product of the reactions of conversion of C_5H_6, C_5H_5, and C_6H_6 to larger aromatic rings.

As anticipated, the change in the performance of the model is mostly related to the increased conversion of phenol. This

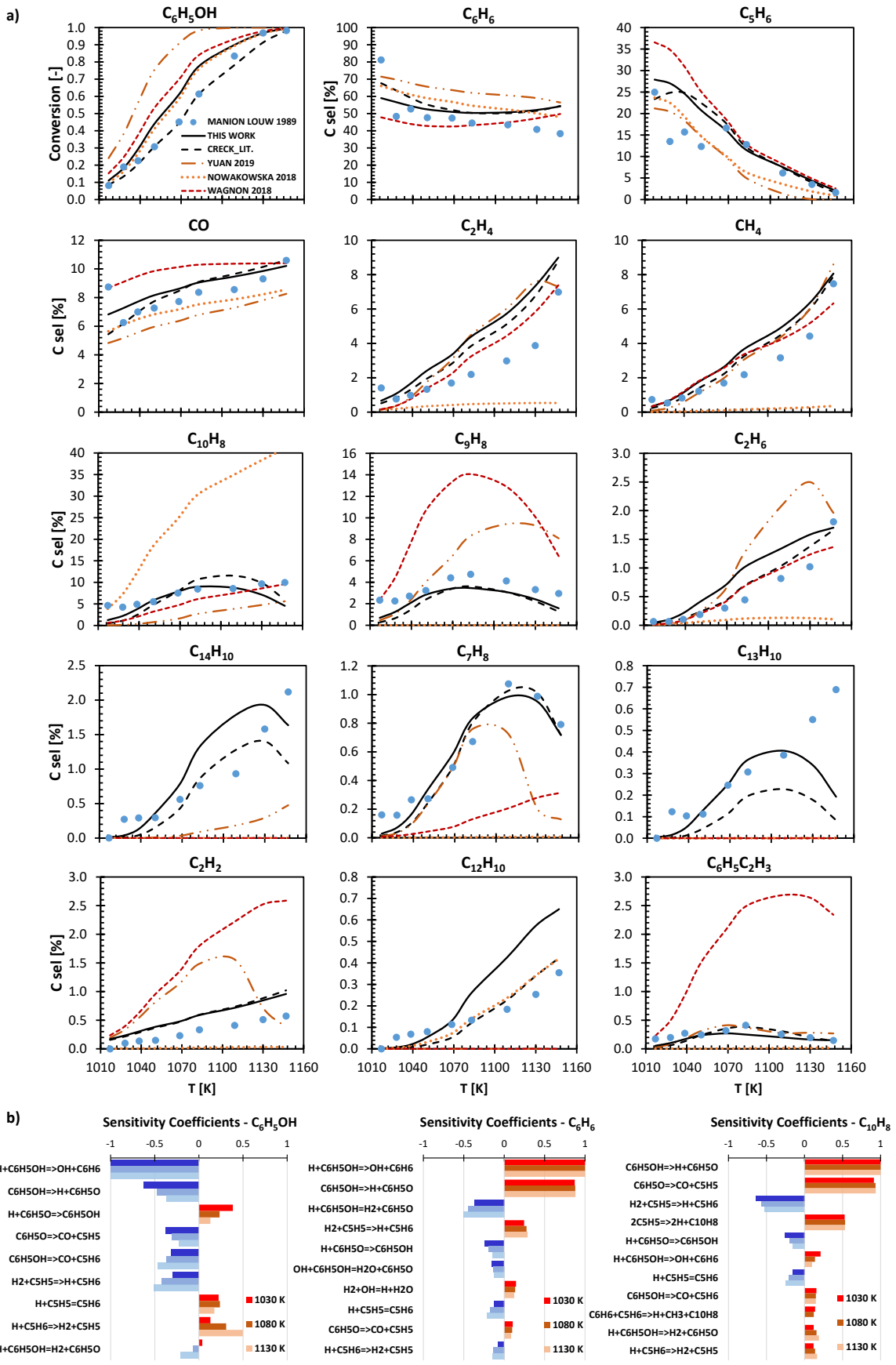

Figure 11: a) Species profiles in terms of carbon selectivity C sel% of the PFR experiments of Manion and Louw (1010-1147 K, 1 atm), b) sensitivities of C_6H_5OH, C_6H_6, and $C_{10}H_8$ at three different temperatures (1030 K, 1080 K, and 1130 K) in the PFR simulated with the updated CRECK kinetic mechanism.

produces an overall higher concentration of H in the system, therefore the relative contribution to the formation of products by the relevant reaction pathways is different. For instance, in the new model CO is produced mainly by the radical decomposition of phenoxy (r_3), whereas in the former model the molecular decomposition (r_1) was mostly responsible for CO concentration. The major modification in terms of carbon selectivity regards the shape of the profile of benzene. This is attributed to the change of C_5H_5 concentration, higher at low conversion and lower at high conversion compared to the previous model. In particular, at low temperature the increased production of C_5H_5 from (r_3) allows it to react with C_6H_6 to form $CH_3 + C_{10}H_8$. The increased concentration of C_5H_6 follows directly from $H_2 + C_5H_5$, whereas in the literature CRECK mechanism (r_5) proceeded in the forward direction as a source of C_5H_5. At high temperatures, the concentration of C_5H_5 is lower than the literature CRECK model due to its higher recombination with H, which largely dominates, contrary to the former model where (r_5) prevailed also at high conversions. Hence, also its consumption with C_6H_6 to larger aromatics is reduced. The shift in the peak of C_5H_5 and the different shape of its profile clearly affect the final concentrations of larger aromatics. A possible future development of the kinetic simulations is the coupling of the CRECK kinetic model with the soot model,[79] so as to test its impact on the predictions of benzene and PAHs.

Among the literature models, the one of Wagnon et al.[12] reproduces reasonably the shape of the profiles of the main products, with a phenol conversion similar to that of the updated CRECK mechanism. Apart from the ipso-addition reaction of H on phenol, also the H-atom abstractions by C_5H_5, indene, and H play an important role. Phenoxy entirely converts to C_5H_5 + CO. C_5H_5 produces C_5H_6 via H-atom abstraction on phenol and recombination with H at high temperatures. C_5H_6 is mostly consumed via addition with H to form C_5H_7 and with C_5H_5 to indene, largely overpredicted by the model also due to shortcomings in the description of indene secondary reactivity. The shape of benzene profile is similar to that predicted by the updated CRECK model. However, at high temperatures C_6H_6 is produced mostly by $H_2 + C_6H_5$, and consumed by addition of C_3H_3 and C_2H_2 to form H + indene and styrene, respectively, contrary to what predicted by the updated CRECK mechanism. The shape of the toluene profile is due to the missing production pathway from indene. Finally, naphthalene is entirely produced from self-recombination of C_5H_5 radicals, though its consumption pathways do not include reactions with H, thus allowing its accumulation in the system. Also the model of Nowakowska et al.[15] predicts a conversion of phenol similar to that of the updated CRECK model, reproducing the trends of the main products (C_6H_6, C_5H_6, CO). Similarly to the mechanism of Wagnon et al.,[12] phenol is consumed by the ipso-addition and H-atom abstraction by H and C_5H_5. Contrary to pyrolysis, the CO profile is in agreement with the experiments thanks to the high concentration of phenoxy radical, which is entirely consumed via decomposition (r_3). C_5H_6 instead is underestimated. In fact, its production from (r_1) and from the recombination of H with C_5H_5 is negligible, as it mostly derives from the H-atom abstraction reaction on phenol by C_5H_5 (similar to Lovell et al.[18]). Overall, the concentration of C_5H_5 is extremely high due to the large formation of phenoxy, so that the production of naphthalene from C_5H_5 recombination is largely overestimated, also considering that no $C_{10}H_8$ consumption via reactions with H is present in the model. Finally, the trend of benzene profile is well reproduced by this mechanism. Only the H ipso-addition on phenol is relevant to its production, and benzene is not consumed significantly by any reaction in the mechanism. Hence, benzene decreases at higher phenol conversion because the higher concentrations of H and C_5H_5 result in a more relevant consumption of phenol via H-atom abstractions by these radicals. Finally, the mechanism of Yuan et al.[74] considerably overestimates the conversion of phenol, despite reproducing the general trends of the carbon selectivity for the main products. Phenol rapidly converts via H ipso-addition, but also via molecular decomposition and H-atom abstraction by C_5H_5, all faster than in the updated CRECK model. Nevertheless, C_5H_6 concentration is as low as in the model of Nowakowska et al.,[15] possibly due to an excessive consumption to C_5H_7 via H addition. It is evident that CO is lower than the experimental profiles due to the favored conversion of phenol to C_6H_6, which is in fact overestimated, though it reproduces the decreasing experimental trend. Similarly to the mechanism of Nowakowska et al.,[15] H ipso-addition on phenol controls its concentration. The polyaromatic rings are formed with reaction pathways similar to those present in the updated CRECK mechanism. However, naphthalene is not consumed via H additions, hence showing monotonic increase with temperature. The reactions leading to larger aromatics also produce smaller by-products and are the main source of C_{1-3} species.

5. Conclusions

We presented a theoretical investigation of relevant reaction pathways to the kinetic mechanism of the pyrolysis of phenol and the oxidation of aromatics. Previous literature studies and sensitivity analyses on the literature CRECK kinetic model highlighted that the relevant channels involved are phenol unimolecular decomposition, phenol bond fission, phenoxy radical decomposition, and H-atom abstractions by H on phenol and cyclopentadiene. The kinetic studies reported in the literature show that there is not yet complete agreement on the detailed mechanism of phenol decomposition, while accurate theoretical calculations of related relevant pathways are still missing. Therefore, we performed high level ab initio based TST-ME calculations to determine accurate temperature and pressure dependent rate constants for the reaction pathways contributing the most to phenol decomposition. We then updated the CRECK kinetic model with our rate constants, and performed kinetic simulations of the available experimental data. Overall, the set of rate constants obtained can be readily implemented in combustion kinetic mechanisms and possibly lead to improvements in the prediction of experimental data for phenol pyrolysis.

Our theoretical investigation of the PES of phenol decomposition only partially confirmed the conclusions of previous literature studies. First, it revealed an unexpected

multi-reference character of the decarbonylation step to the products, which lowers the TS barrier by almost 4 kcal mol^{-1} with respect to the CCSD(T)/CBS value. The rate constant obtained for (r_1) is in general agreement with previous theoretical and experimental studies, being about half the value obtained by Xu and Lin.[25] Our calculations also highlighted the contribution of C-H bond fissions from the 2,4-C_6H_6O and 2,5-C_6H_6O intermediates to the formation of phenoxy radical. The global rate constant of phenoxy formation (r_2) is thus twice the one previously used in the CRECK mechanism. Hence, molecular decomposition of phenol to CO and C_5H_6 dominates over bond fission to phenoxy radical only below ~1400 K. The competition between (r_1) and (r_2) determines the main mechanism of formation of CO. At lower temperature, the molecular decomposition largely controls the profile of CO, as in the PFR experiments of Brezinsky et al.[17] (1173 K). On the other hand, in the ST experiments of Horn et al.[19] (1477 K, 1536 K) phenol is mostly consumed by (r_2), although (r_1) still contributes significantly to the reactivity. Phenoxy radical then decomposes by (r_3), producing CO. The increased relevance of (r_2) with respect to what predicted by the literature CRECK kinetic model leads to a higher concentration of H in the system, which improves the simulated C_6H_6 and H profiles of these experimental data sets.[17,19]

At high temperatures, the formation of phenoxy and H radicals becomes significant. Hence, the radical decomposition of phenoxy to CO + C_5H_5 (r_3) and the H-atom abstractions by H on both phenol (r_4) and cyclopentadiene (r_5) gain relevance in the kinetic mechanism. As regards the decomposition of phenoxy, the available experimental and theoretical data are widely scattered, due to the influence of secondary reactivity of the precursors of phenoxy (in experiments) and the impact of the theoretical methodology on the final rate (in calculations). We found reasonable agreement with the rate constants proposed by Frank et al.[32] and more recently by Shu et al.[33] In our PES study, we also included the isomerization of phenoxy to o,m,p-C_6H_4OH. As stated by Hemberger et al.,[71] only the meta and para isomers may stabilize in pyrolysis conditions, whereas the ortho isomer converts fast to phenoxy. Our ME simulations confirmed that m,p-C_6H_4OH form only at high temperatures, and then convert directly to CO + C_5H_5. However, we obtained equivalent results in kinetic simulations of reactor experiments of phenol pyrolysis excluding the unimolecular reactivity of o,m,p-C_6H_4OH, hence we did not include it in the updated CRECK mechanism. These radicals may instead affect the reactivity significantly in the presence of high concentrations of radicals, as found in oxidation systems.[52] As far as the H-atom abstractions by H on phenol is concerned, we found general agreement with former experimental and theoretical studies.[37,39] This is also the first theoretical work where abstractions on the phenolic ring are explicitly considered. As for the H-atom abstraction on cyclopentadiene, we found good agreement with recently calculated values,[45,73] though the rate constant is significantly lower than the one previously used in the CRECK mechanism. This strongly impacts the concentration of H in both pyrolysis, resulting in a better agreement of the H profile with the experimental data,[19] and in hydrogenolysis, increasing the concentration of C_5H_6 at low conversions of phenol.[21] However, in the latter case the lower consumption of H radical is the main cause, together with the increased phenoxy radical decomposition and phenol bond fission ($r_{2,3}$), of the overprediction of phenol conversion. This causes also an increase in the concentrations of C_{1-3} species with respect to experiments.

The accuracy of our calculations is supported by the overall agreement between the simulations with the updated CRECK kinetic mechanism and the experimental data[17,19,21] for the profiles of the main species (phenol, CO, C_5H_6, H). Nevertheless, there is still room for improvement as regards the secondary products. Our sensitivity analysis on pyrolysis simulations[17,19] highlighted the relevance of the interaction of both phenol and cyclopentadiene with the OH radical (initially formed via H ipso-addition on phenol). In particular, accurate theoretical studies of the H-atom abstractions by OH and OH additions to C_5H_6 are still missing. A more significant consumption of OH would also help to foster H ipso-addition to phenol, thus increasing the concentration of C_6H_6, and possibly find a source of CH_3 radicals, still underpredicted by the model. As regards the thermolysis of phenol in the presence of hydrogen, the model still requires improvement in terms of the competition between the formation of PAHs by C_5H_6 and C_5H_5 and their decomposition to smaller radicals. It might be useful to both integrate in the model recent investigations of low temperature PAH formation[80,81] and to consider H addition to C_5H_6 to form C_5H_7, currently not included in the CRECK kinetic model. Furthermore, the integration of the kinetics of soot formation in the final model might also have an impact on the simulated PAH profiles.[79] Finally, considering the lack of data on the pyrolysis and oxidation of phenol, additional experimental investigations would indeed contribute to understanding further the complex kinetic mechanism of this system. We believe this work also provides a solid basis for future theoretical investigations of phenolic species oxidation.

Conflicts of interest

There are no conflicts to declare.

Acknowledgements

This work is supported by The Computational Chemistry Consortium (C3). The C3 Team gratefully acknowledges the support of the industry funding members of C3 consortium.

References

1 G. Vourliotakis, G. Skevis and M. A. Founti, *Energy and Fuels*, 2011, **25**, 1950–1963.

2 C. Saggese, A. Frassoldati, A. Cuoci, T. Faravelli and E. Ranzi, *Combust. Flame*, 2013, **160**, 1168–1190.

3 S. Fascella, C. Cavallotti, R. Rota and S. Carrà, *J. Phys. Chem.*

A, 2004, **108**, 3829–3843.
4 D. Wang, A. Violi, D. H. Kim and J. A. Mullholland, *J. Phys. Chem. A*, 2006, **110**, 4719–4725.
5 V. V Kislov and A. M. Mebel, *J. Phys. Chem. A*, 2007, **111**, 9532–9543.
6 C. Cavallotti, D. Polino, A. Frassoldati and E. Ranzi, *J. Phys. Chem. A*, 2012, **116**, 3313–3324.
7 M. R. Djokic, K. M. Van Geem, C. Cavallotti, A. Frassoldati, E. Ranzi and G. B. Marin, *Combust. Flame*, 2014, **161**, 2739–2751.
8 T. Faravelli, A. Frassoldati, G. Migliavacca and E. Ranzi, *Biomass and Bioenergy*, 2010, **34**, 290–301.
9 P. R. Patwardhan, R. C. Brown and B. H. Shanks, *ChemSusChem*, 2011, **4**, 1629–1636.
10 C. Mukarakate, A. M. Scheer, D. J. Robichaud, M. W. Jarvis, D. E. David, G. B. Ellison, M. R. Nimlos and M. F. Davis, *Rev. Sci. Instrum.*, 2011, **82**, 033104.
11 S. Van Den Bosch, W. Schutyser, R. Vanholme, T. Driessen, S. F. Koelewijn, T. Renders, B. De Meester, W. J. J. Huijgen, W. Dehaen, C. M. Courtin, B. Lagrain, W. Boerjan and B. F. Sels, *Energy Environ. Sci.*, 2015, **8**, 1748–1763.
12 S. W. Wagnon, S. Thion, E. J. K. Nilsson, M. Mehl, Z. Serinyel, K. Zhang, P. Dagaut, A. A. Konnov, G. Dayma and W. J. Pitz, *Combust. Flame*, 2018, **189**, 325–336.
13 M. Pelucchi, C. Cavallotti, A. Cuoci, T. Faravelli, A. Frassoldati and E. Ranzi, *React. Chem. Eng.*, 2019, **4**, 490–506.
14 M. Nowakowska, O. Herbinet, A. Dufour and P.-A. Glaude, *Combust. Flame*, 2014, **161**, 1474–1488.
15 M. Nowakowska, O. Herbinet, A. Dufour and P. A. Glaude, *J Phys Chem A*, 2018, **122**, 7894–7909.
16 E. Ranzi, M. Costa, M. Pelucchi, T. Faravelli, A. Frassoldati, G. Sribala, G. B. Marin and K. M. Van Geem, in *Chemical Engineering Transactions*, 2018, vol. 65.
17 K. Brezinsky, M. Pecullan and I. Glassman, *J. Phys. Chem. A*, 1998, **102**, 8614–8619.
18 A. B. Lovell, K. Brezinsky and I. Glassman, *Int. J. Chem. Kinet.*, 1989, **21**, 547–560.
19 C. Horn, K. Roy, P. Frank and T. Just, in *Symposium (International) on Combustion*, 1998, pp. 321–328.
20 M. U. Alzueta, P. Glarborg and K. Dam-Johansen, *Int. J. Chem. Kinet.*, 2000, **32**, 498–522.
21 J. A. Manion and R. Louw, *J. Phys. Chem*, 1989, **93**, 3563–3574.
22 J. A. Manion and R. Louw, *J. Phys. Chem.*, 1990, **94**, 4127–4134.
23 L. Khachatryan, J. Adounkpe and B. Dellinger, *J Phys Chem A*, 2008, **112**, 481–487.
24 L. Zhu and J. W. Bozzelli, *J Phys Chem A*, 2003, **107**, 3696–3703.
25 Z. F. Xu and M. C. Lin, *J. Phys. Chem. A*, 2006, **110**, 1672–1677.
26 A. M. Scheer, C. Mukarakate, D. J. Robichaud, M. R. Nimlos, H.-H. Carstensen and G. B. Ellison, *J. Chem. Phys*, 2012, **136**, 44309.
27 A. Ristori, P. Dagaut, A. El Bakali, G. Pengloan and M. Cathonnet, *Combust. Sci. Technol.*, 2001, **167**, 223–256.
28 B. SirJean and R. Fournet, *J. Phys. Chem. A*, 2012, **116**, 6675–6684.
29 A. J. Colussi, F. Zabel and S. W. Benson, *Int. J. Chem. Kinet.*, 1977, **9**, 161–178.
30 C.-Y. Lin and M. C. Lin, *Int. J. Chem. Kinet.*, 1985, **17**, 1025–1028.
31 C. Y. Lin and M. C. Lin, *J. Phys. Chem.*, 1986, **90**, 425–431.
32 P. Frank, J. Herzler, T. H. Just and C. Wahl, *Symp. Combust.*, 1994, **25**, 833–840.
33 B. Shu, J. Herzler, S. Peukert, M. Fikri and C. Schulz, *Int. J. Chem. Kinet.*, 2017, **49**, 656–667.
34 S. Olivella, A. Solé and A. Garcìa-Raso, *J. Phys. Chem*, 1995, **99**, 10549–10556.
35 R. Liu, K. Morokuma, A. M. Mebel and M. C. Lin, *J. Phys. Chem.*, 1996, **100**, 9314–9322.
36 H.-H. Carstensen and A. M. Dean, *Int. J. Chem. Kinet. - Spec. Issue 7th Int. Conf. Chem. Kinet.*, 2012, **44**, 75–89.
37 Y. Z. He, W. G. Mallard and W. Tsang, *J. Phys. Chem.*, 1988, **92**, 2196–2201.
38 Q. Zhang, X. Qu, H. Wang, F. Xu, X. Shi and W. Wang, *Environ. Sci. Technol.*, 2009, **43**, 4105–4112.
39 R. A. Shandross, J. P. Longwell and J. B. Howard, *Twenty-Sixth Symp. Combust.*, 1996, **26**, 711–719.
40 J. H. Kiefer, L. J. Mizerka, M. R. Patel and H.-C. Wei, *A Shock Tube Investigation of Major Pathways in the High-Temperature Pyrolysis of Benzene*, 1985, vol. 89.
41 A. M. Dean, *J. Phys. Chem*, 1990, **94**, 1432–1439.
42 X. Zhong and J. W. Bozzelli, *Int. J. Chem. Kinet.*, 1997, **29**, 893–913.
43 K. Roy, P. Frank and T. Just, *Isr. J. Chem.*, , DOI:10.1002/ijch.199600038.
44 G. B. Bacskay, M. Martoprawiro and J. C. Mackie, *Chem. Phys. Lett.*, 1998, **290**, 391–398.
45 L. V. Moskaleva and M. C. Lin, *Proc. Combust. Inst.*, 2002, **29**, 1319–1327.
46 C. Cavallotti, M. Pelucchi, Y. Georgievskii and S. J. Klippenstein, *J. Chem. Theory Comput.*, 2019, **15**, 1122.
47 M. Frisch, G. Trucks, H. B. Schlegel, G. E. Scuseria, M. A. Robb, J. R. Cheeseman, G. Scalmani and V. Barone, 2009.
48 H. J. Werner, P. Knowles, R. Lindh, F. R. Manby, M. Schütz, P. Celani, T. Korona, G. Rauhut, R. Amosand and A. Bernhardsson, 2010.
49 S. J. Klippenstein and J. A. Miller, *J. Phys. Chem. A*, 2002, **106**, 9267–9277.
50 J.-D. Chai and M. Head-Gordon, *Phys. Chem. Chem. Phys.*, 2008, **10**, 6615.
51 Y. Zhao and D. G. Truhlar, *Theor. Chem. Acc.*, 2008, **120**, 215–241.
52 M. Pelucchi, C. Cavallotti, T. Faravelli and S. J. Klippenstein, *Phys. Chem. Chem. Phys.*, 2018, **20**, 10607–10627.
53 M. Urban, J. Noga, S. J. Cole and R. J. Bartlett, *J. Chem. Phys.*, 1985, **83**, 4041–4046.
54 J. M. L. Martin, *Chem. Phys. Lett.*, 1996, **259**, 669–678.
55 H.-J. Werner, *Mol. Phys.*, 1996, **89**, 645–661.
56 P. Celani and H.-J. Werner, *J. Chem. Phys.*, 2000, **112**, 5546–5557.
57 T. J. Lee and P. R. Taylor, *Int. J. Quantum Chem. Quantum*

Chem. Symp. 23, 1989, 199–207.
58 A. Karton, E. Rabinovich, J. M. L. Martin and B. Ruscic, *J. Chem. Phys.*, 2006, **125**, 144108.
59 O. Tishchenko, J. Zheng and D. G. Truhlar, *J. Chem. Theory Comput.*, 2008, **4**, 1208–1219.
60 G. Ghigo and O. Roos, *Chem. Phys. Lett.*, 2004, **396**, 142–149.
61 S. Sharma, S. Raman and W. H. Green, *J. Phys. Chem. A*, 2010, **114**, 5689–5701.
62 C. Eckart, *Phys. Rev.*, 1930, **35**, 1303–1309.
63 J. A. Miller and S. J. Klippenstein, *J. Phys. Chem. A*, 2006, **110**, 10528–10544.
64 D. C. Tardy and B. S. Rabinovitch, *J. Chem. Phys.*, 1966, **45**, 3720–3730.
65 A. Cuoci, A. Frassoldati, T. Faravelli and E. Ranzi, *Comput. Phys. Commun.*, 2015, **192**, 237–264.
66 B. Ruscic and D. H. Bross, Active Thermochemical Tables (ATcT) values based on ver. 1.122d of the Thermochemical Network Argonne National Laboratory (2018); available at ATcT.anl.gov.
67 C. A. Grambow, A. Jamal, Y.-P. Li, W. H. Green, † Judit, Z. Zádor and Y. V Suleimanov, *J. Am. Chem. Soc.*, 2018, **140**, 1035–1048.
68 S. G. Davis, H. Wang, K. Brezinsky and C. K. Law, in *Twenty-Sixth Symposium (International) on Combustion*, 1996, pp. 1025–1033.
69 J. M. Simmie and K. P. Somers, *J. Phys. Chem. A*, 2015, **119**, 7235−7246.
70 X. You, † Dmitry, Y. Zubarev, W. A. Lester and M. Frenklach, *J. Phys. Chem. A*, 2011, **115**, 14184–14190.
71 P. Hemberger, G. da Silva, A. J. Trevitt, T. Gerber and A. Bodi, *Phys. Chem. Chem. Phys.*, 2015, **17**, 30076–30083.
72 M. B. Prendergast, B. B. Kirk, J. D. Savee, D. L. Osborn, C. A. Taatjes, K.-S. Masters, S. J. Blanksby, G. da Silva and A. J. Trevitt, *Phys. Chem. Chem. Phys.*, 2016, **18**, 4320–4332.
73 B. Sirjean, R. Fournet, P.-A. Glaude, ́Frédérique Battin-Leclerc, W. Wang and M. A. Oehlschlaeger, *J. Phys. Chem. A*, 2013, **117**, 1371–1392.
74 W. Yuan, T. Li, Y. Li, M. Zeng, Y. Zhang, J. Zou, C. Cao, W. Li, J. Yang and F. Qi, *Combust. Flame*, 2019, **201**, 187–199.
75 F. Dubnikova and A. Lifshitz, *J Phys Chem A*, 2002, **106**, 8173–8183.
76 A. Lifshitz, C. Tamburu, A. Suslensky and F. Dubnikova, *Proc. Combust. Inst.*, 2005, **30**, 1039–1047.
77 L. B. Harding, S. J. Klippenstein and Y. Georgievskii, *J. Phys. Chem. A*, 2007, **111**, 3789–3801.
78 M. Frenklach, R. I. Singh and A. M. Mebel, *Proc. Combust. Inst.*, 2019, **37**, 969–976.
79 W. Pejpichestakul, E. Ranzi, M. Pelucchi, A. Frassoldati, A. Cuoci, A. Parente and T. Faravelli, *Proc. Combust. Inst.*, , DOI:10.1016/j.proci.2018.06.104.
80 A. E. Long, S. S. Merchant, A. G. Vandeputte, H.-H. Carstensen, A. J. Vervust, G. B. Marin, K. M. Van Geem and W. H. Green, *Combust. Flame*, 2018, **187**, 247–256.
81 A. J. Vervust, M. R. Djokic, S. S. Merchant, H.-H. Carstensen, A. E. Long, G. B. Marin, W. H. Green and K. Van Geem, *Energy & Fuels*, 2018, **32**, 3920–3934.